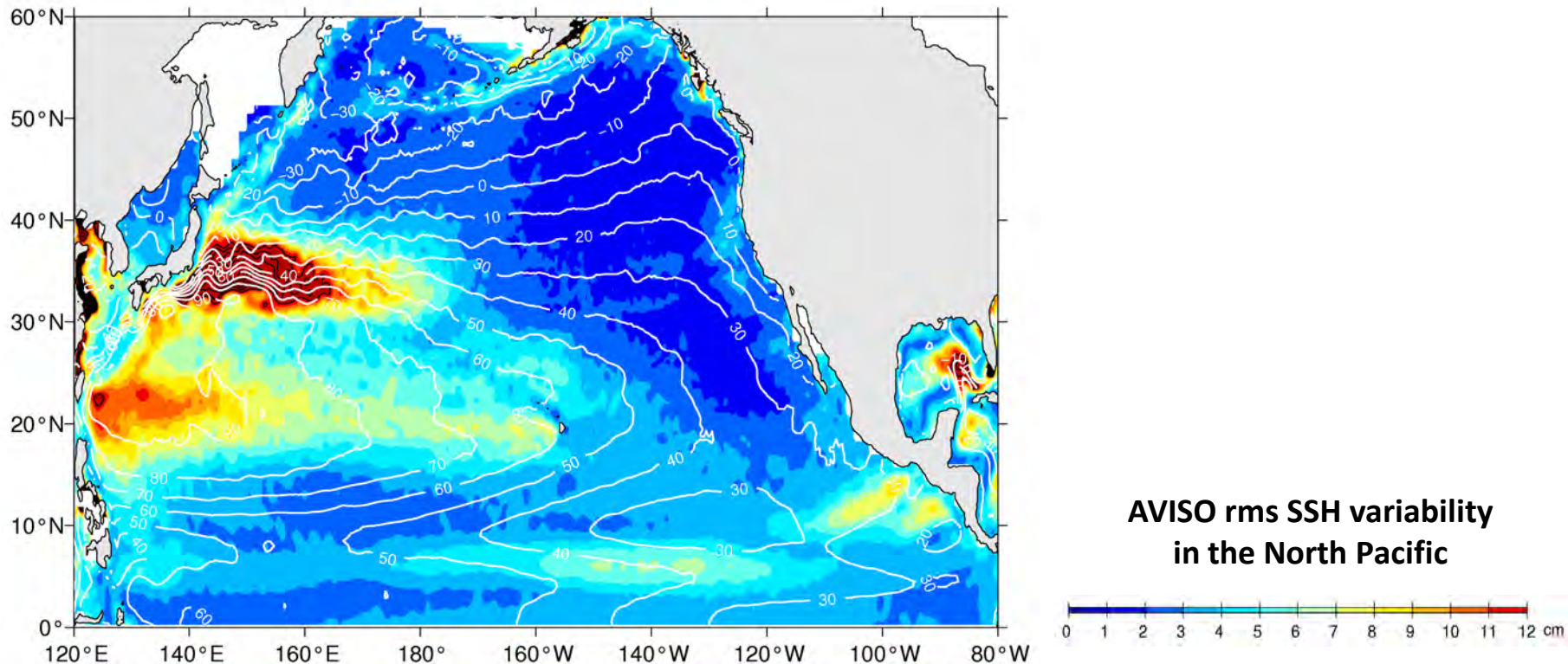


Oceanic Variability from Mesoscale to Submesoscale

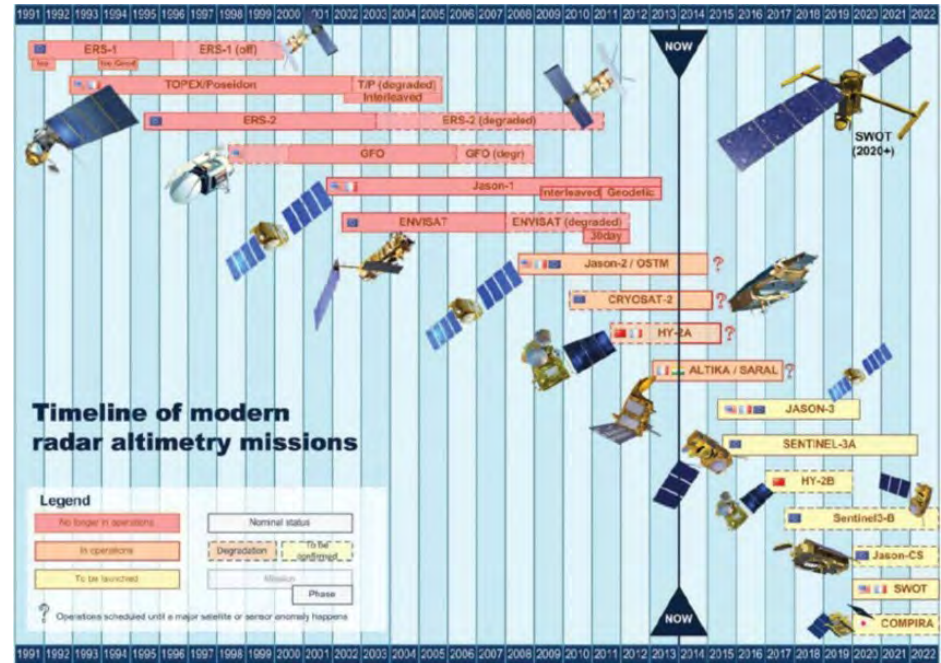
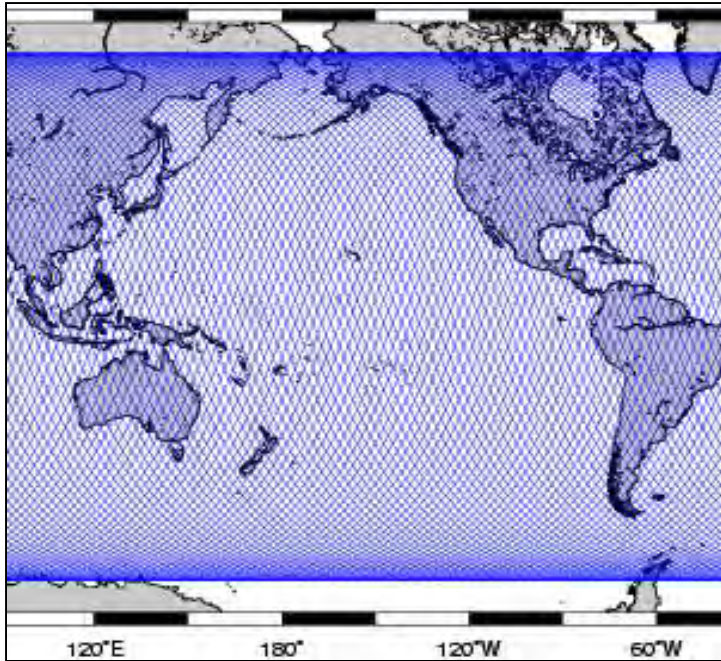
-- Dynamics, Opportunities & Challenges

Bo Qiu (Department of Oceanography, University of Hawaii)

Collaborators: S. Chen (UH), P. Klein (JPL), H. Sasaki (JAMSTEC), Y. Sasai (JAMSTEC),
T. Nakano (JMA), J. Wang (JPL), L. Fu (JPL), D. Menemenlis (JPL)



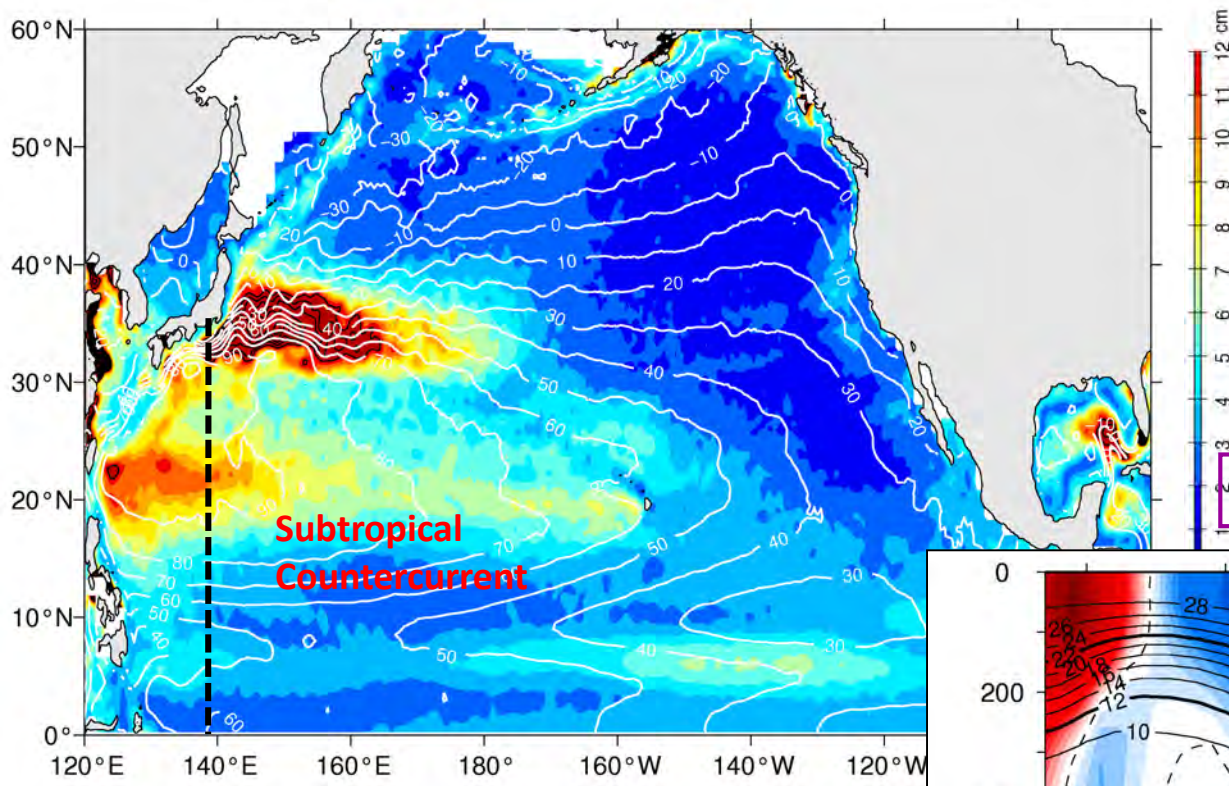
Satellite altimetry missions & their typical ground tracks



Le Traon et al. (2015, JOO)

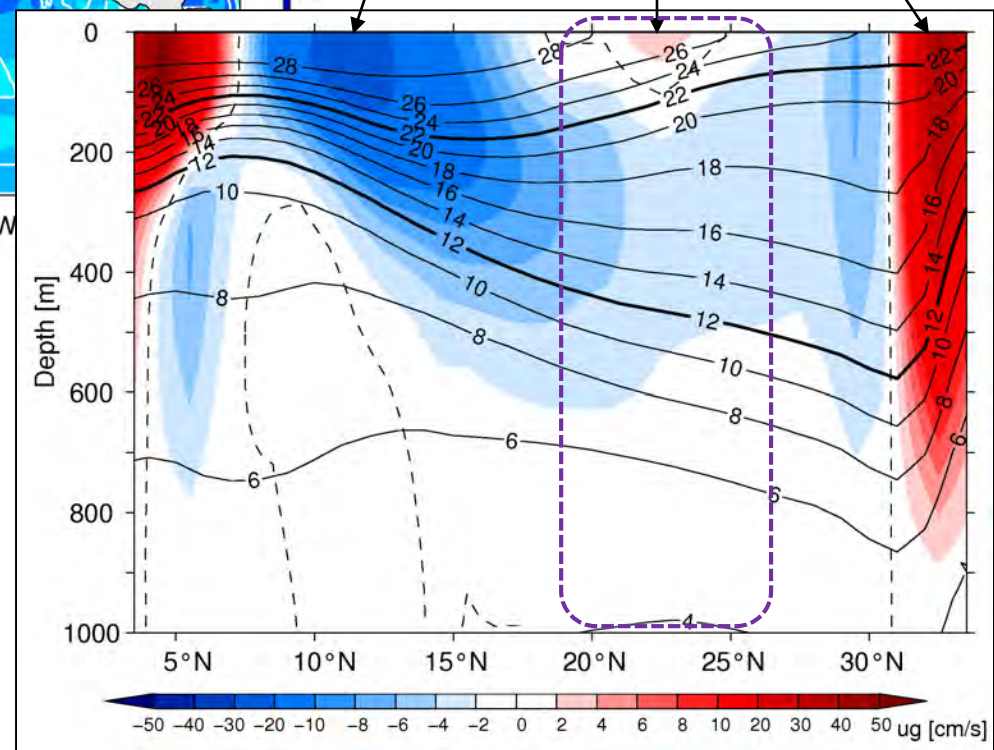
- Ground track separation at equator is ~ 135 km with an exact repeat cycle of 9.9 days
- Multiple concurrent missions have been achieved since 1993
- With 2-3 missions, the resolved oceanic features (by, e.g., the weekly AVISO product) are on the order of **100-150 km**

Time-mean STCC is generated by convergent Ekman heat fluxes in upper ocean

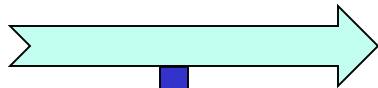


JMA temperature and Ug section along 137°E (1993-2008 mean)

NEC STCC Kuroshio



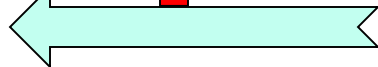
mid-latitude westerly winds



cold Ekman flux

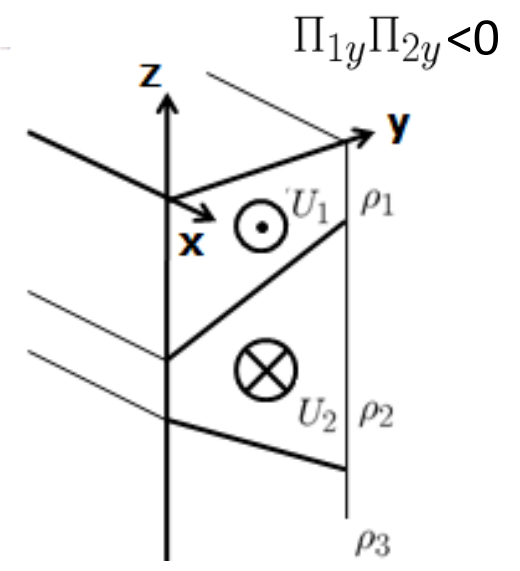
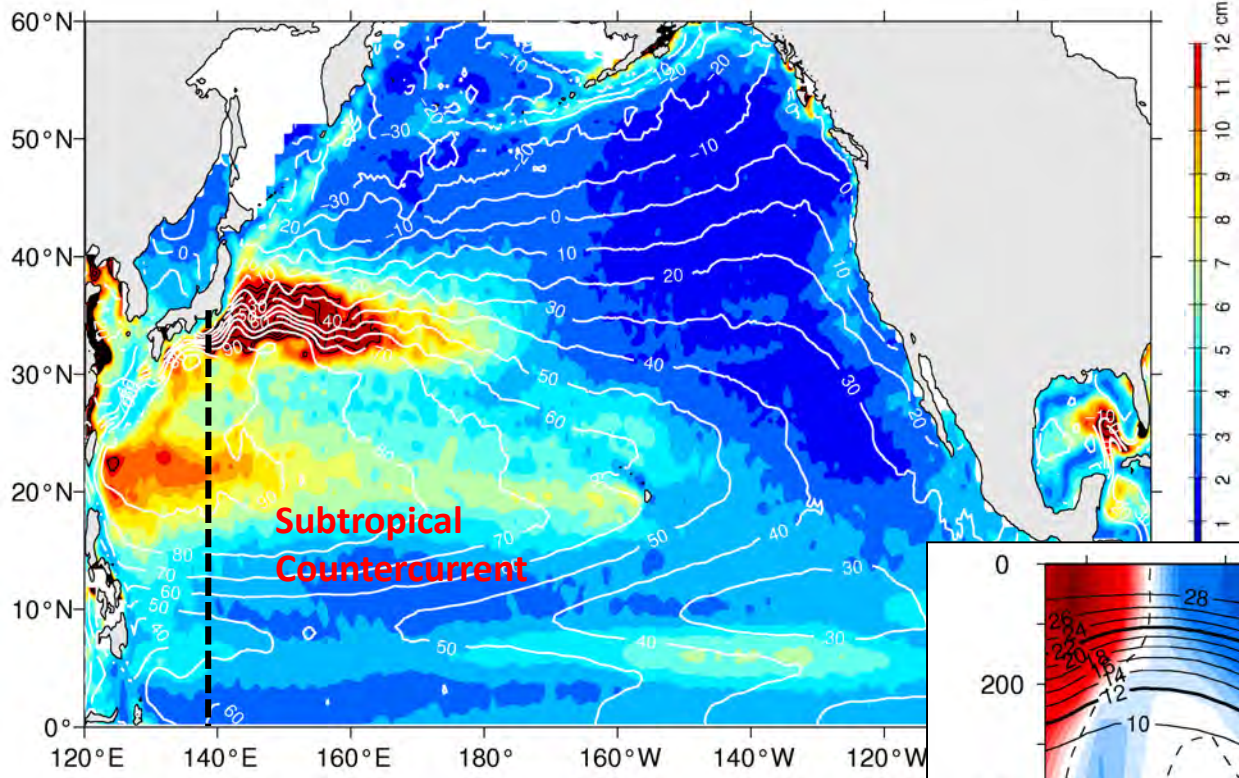


warm Ekman flux

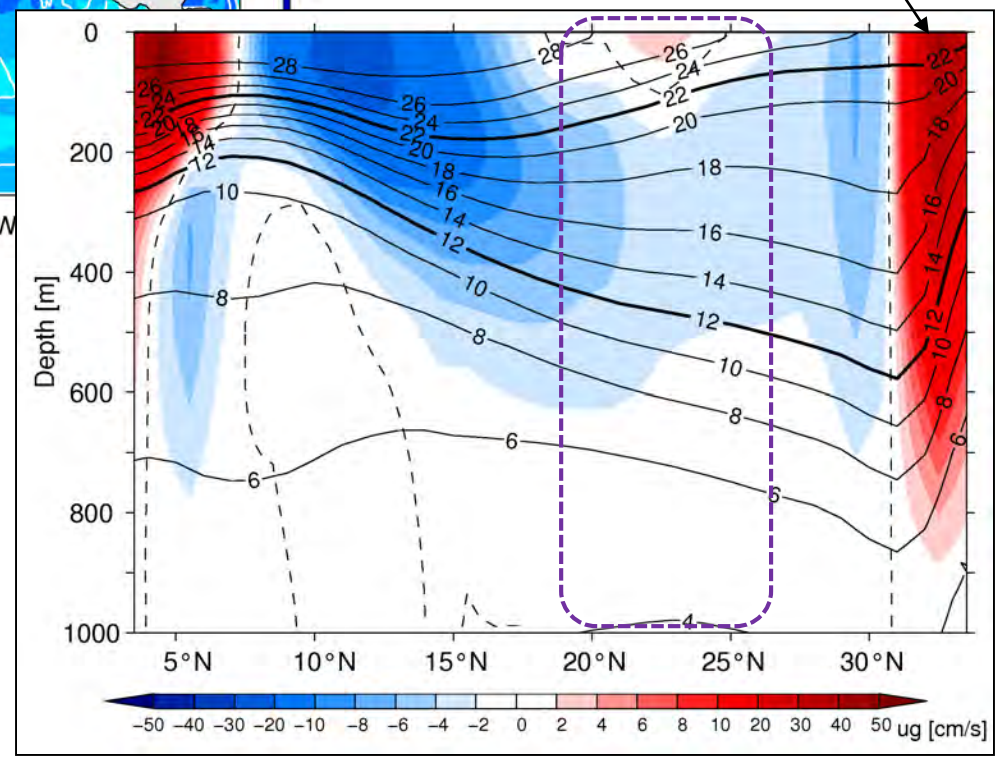


tropical trade winds

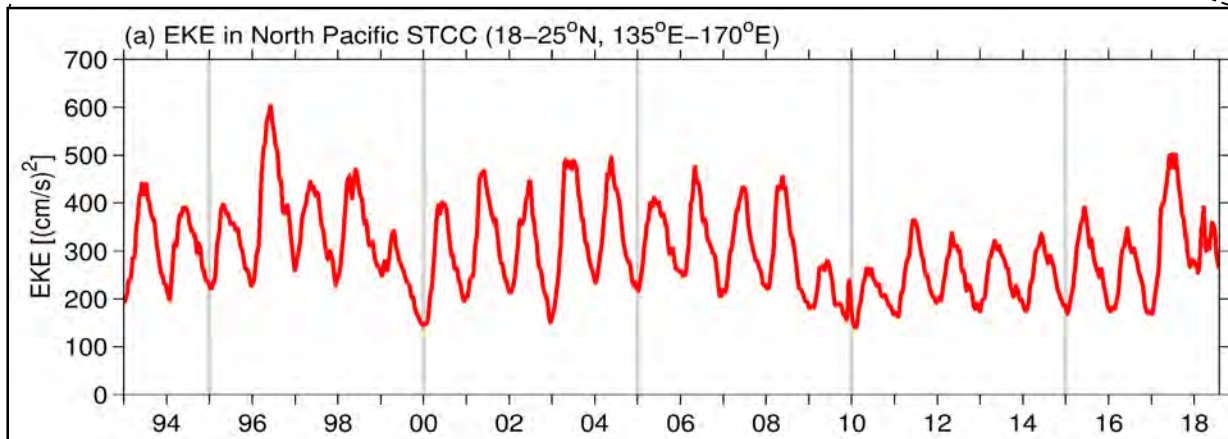
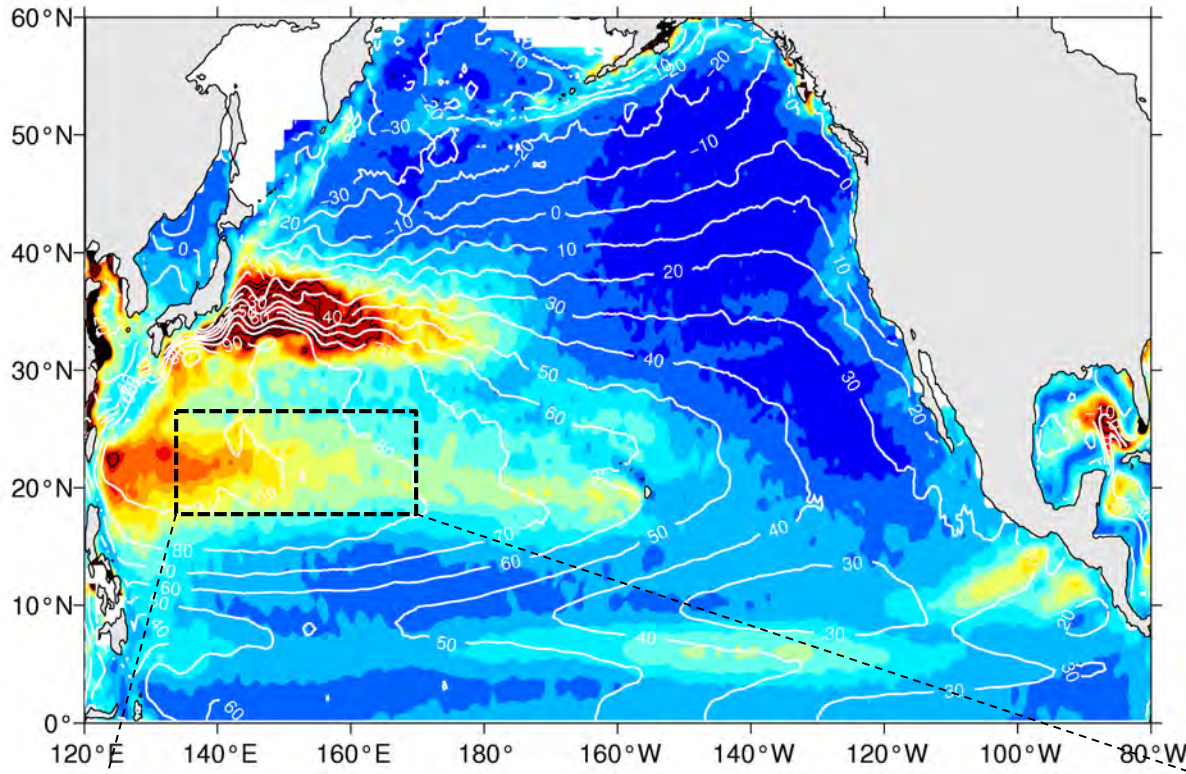
STCC band has the **2nd highest EKE** level in the North Pacific



Meridional PV gradient in the upper seasonal thermocline has **opposite sign** to that in the lower main thermocline, satisfying the condition for **baroclinic instability**



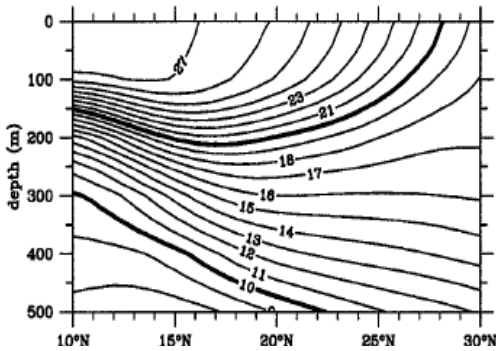
AVISO-based EKE time series in the STCC band: 18°-25°N, 135°-170°E



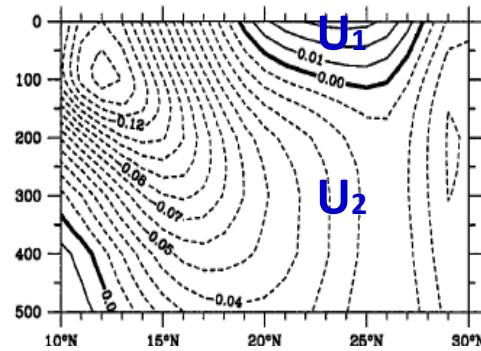
- well-defined annual EKE cycle: May max & January min

T(y,z) & U(y,z) in March vs. September

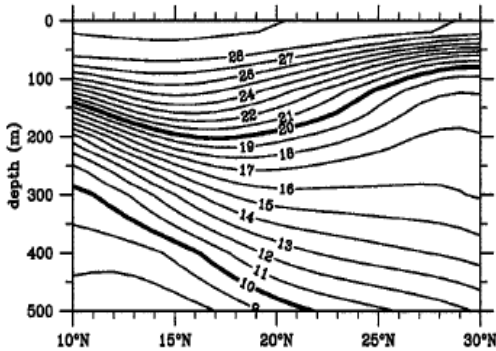
(a) T(y,z) in March



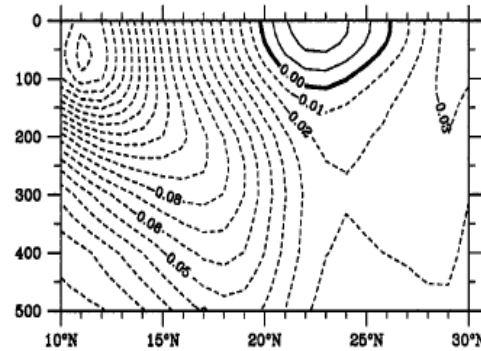
U(y,z) in March



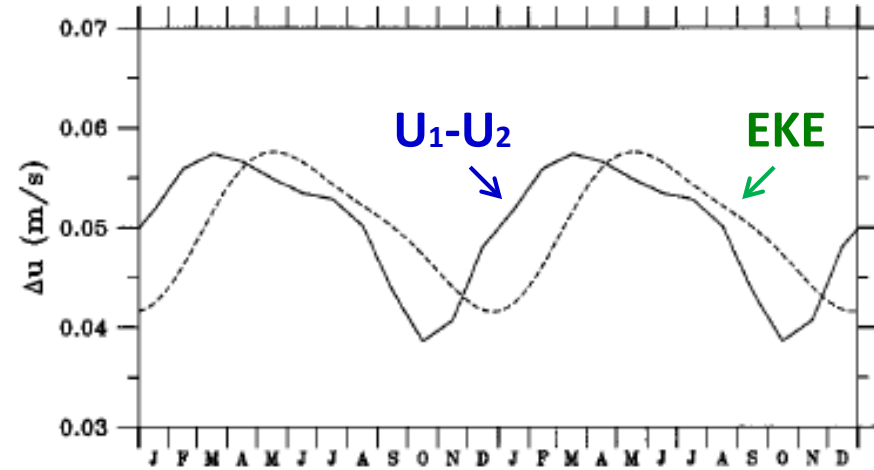
(c) T(y,z) in September



U(y,z) in September

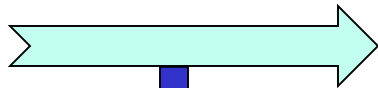


Annual cycle of U₁-U₂ vs. EKE



- **March: stronger STCC/NEC shear + weaker surface N^2**
- **Mean flow shear annual cycle leads that of EKE by ~ 2 months**

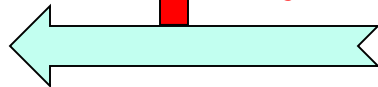
mid-latitude westerly winds



cold Ekman flux

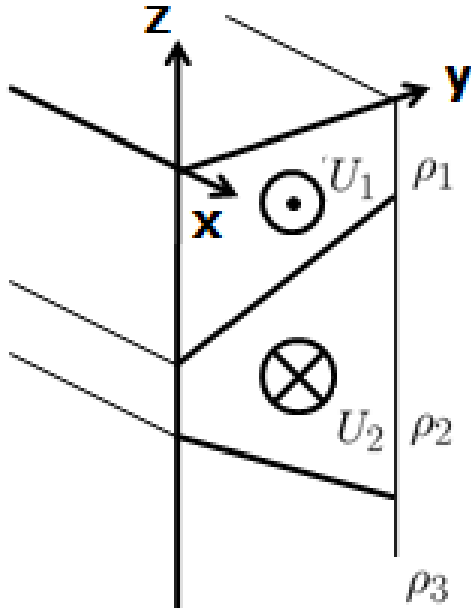


warm Ekman flux

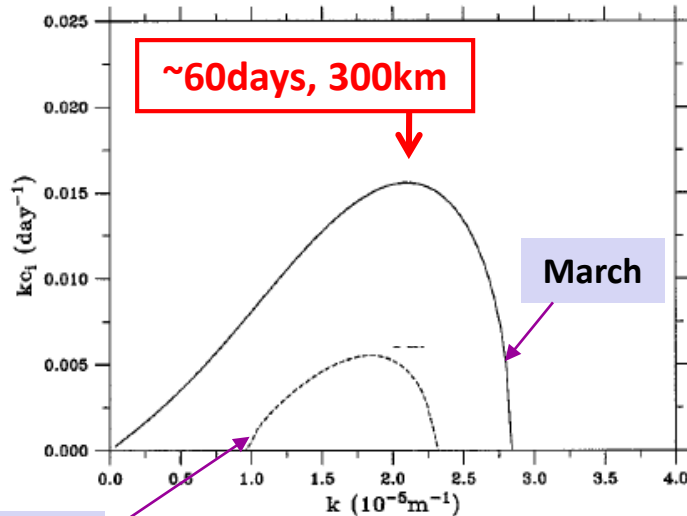
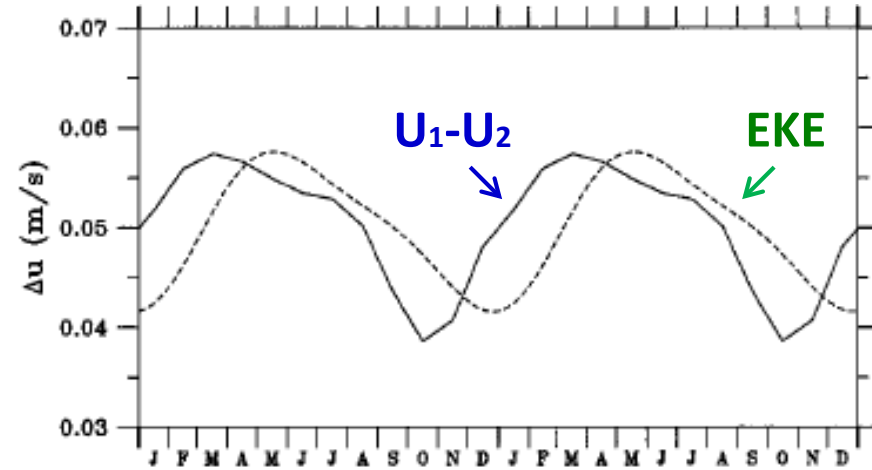


tropical trade winds

Sheared STCC-NEC system in a 2.5-layer RG model



Annual cycle of U_1-U_2 vs. EKE



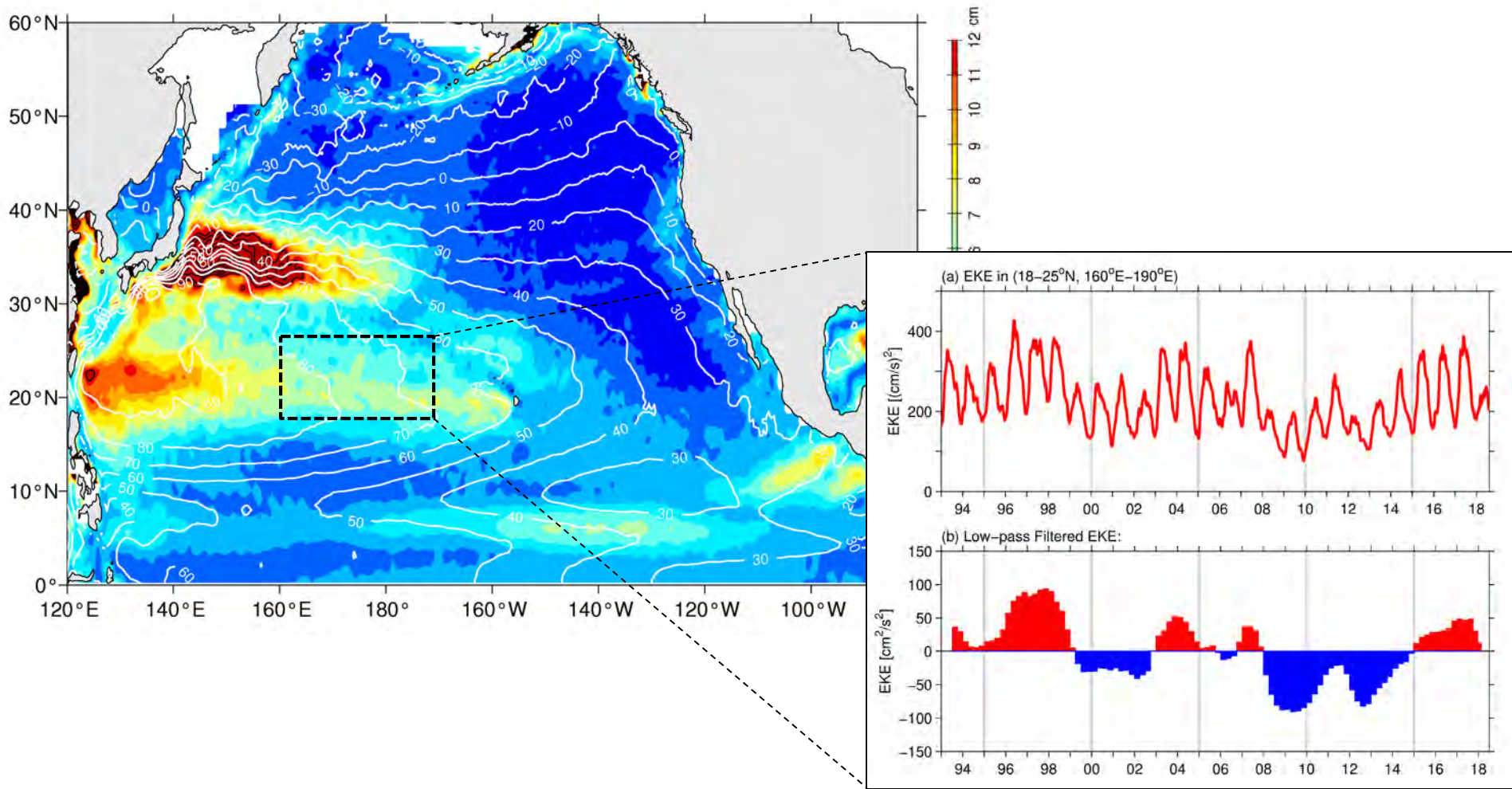
growth rate

September

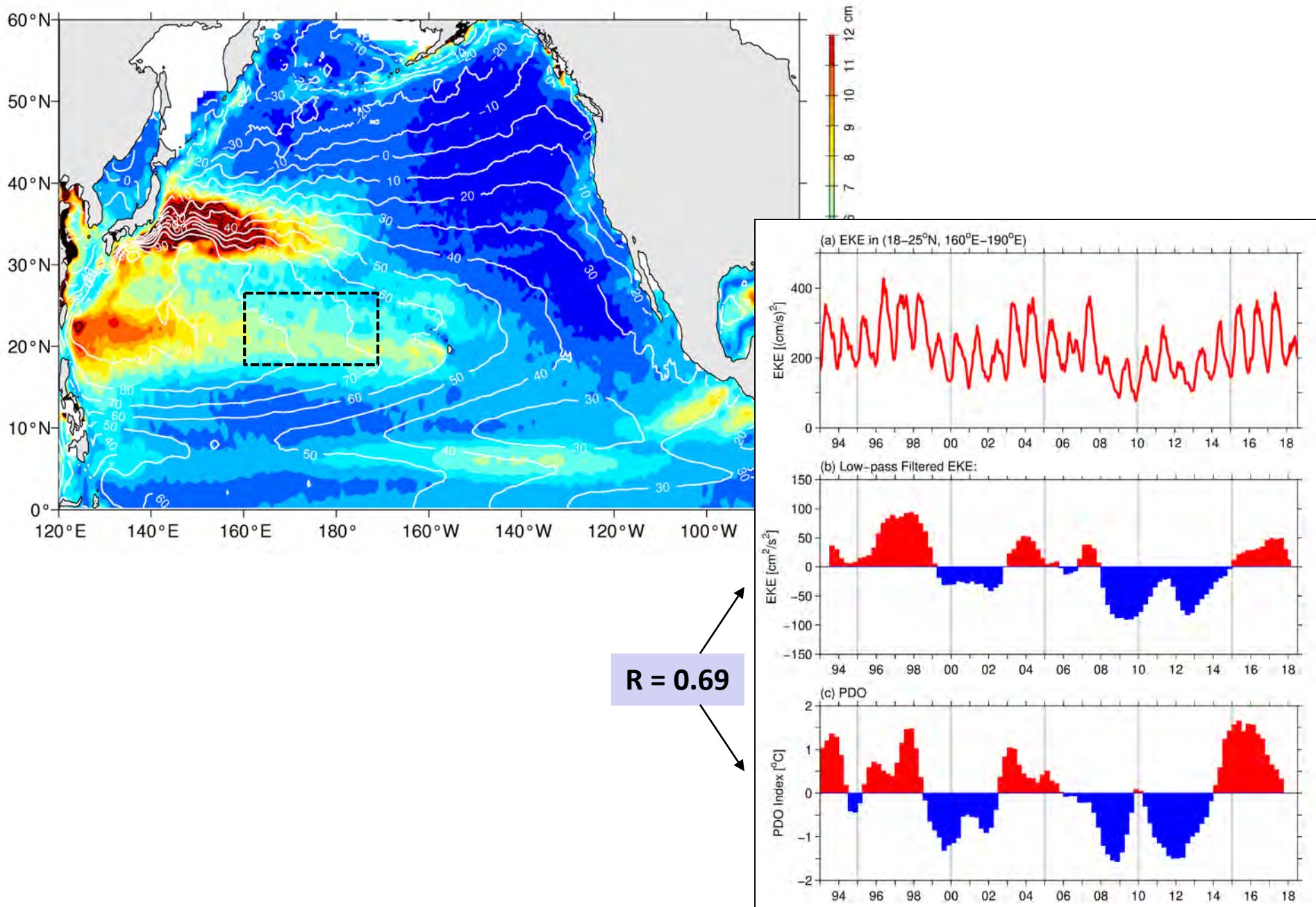
- **March: stronger STCC/NEC shear + weaker surface N^2**
- Mean flow shear annual cycle leads that of EKE by ~ 2 months
- 2.5-layer model predicts an e-folding growth scale of ~ 60 days, explaining the 2-month EKE delay behind U_1-U_2

Qiu (1999, JPO)

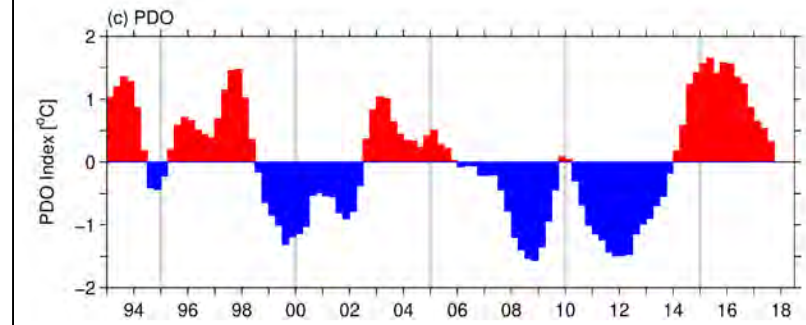
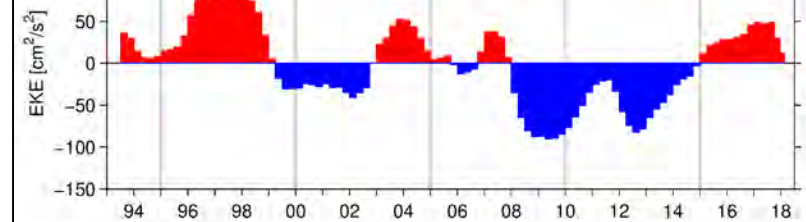
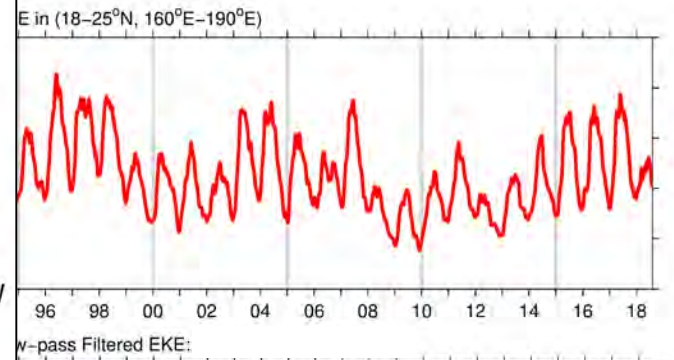
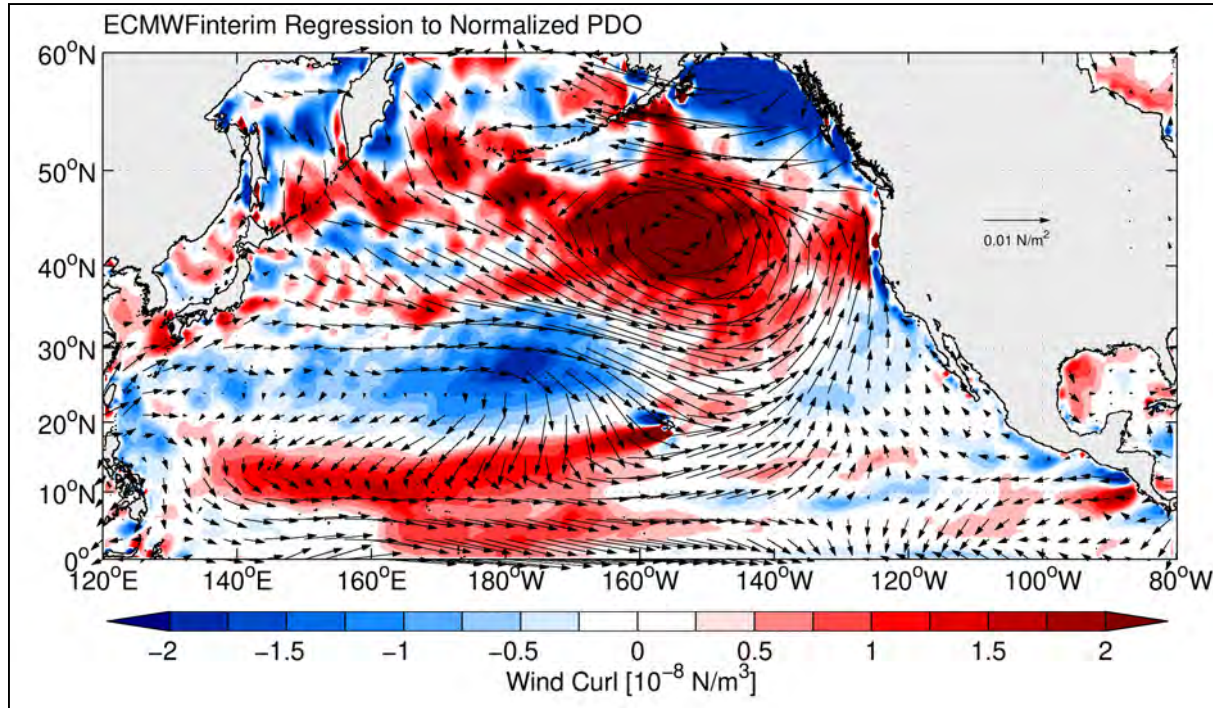
STCC's EKE level also has prominent interannual-decadal modulations



STCC's low-frequency EKE variability corresponds well to the PDO index



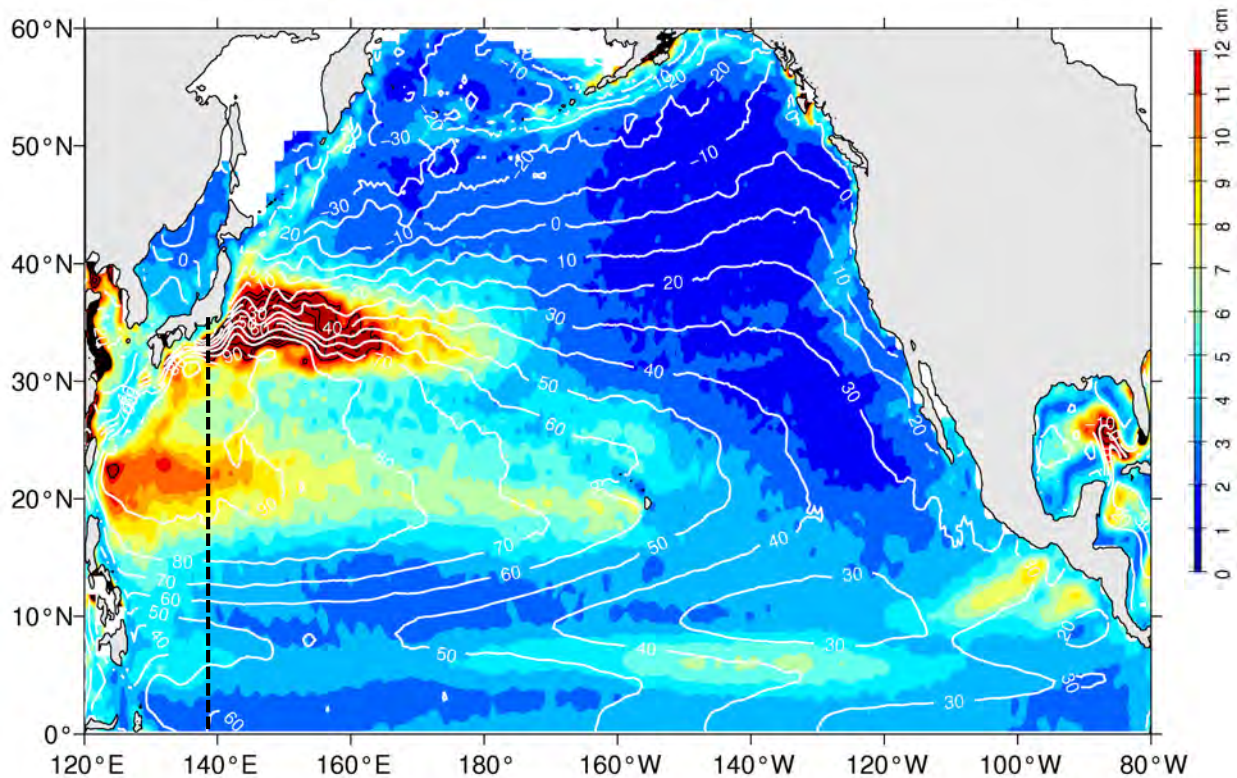
Wind stress vector & curl (in color) regressed to the PDO index



- When PDO index is positive, both trades & westerlies intensify, enhancing Ekman temperature flux convergence along STCC
- This increases **STCC's baroclinicity** & results in more intense instability & eddy generation

Qiu & Chen (2013, JPO)

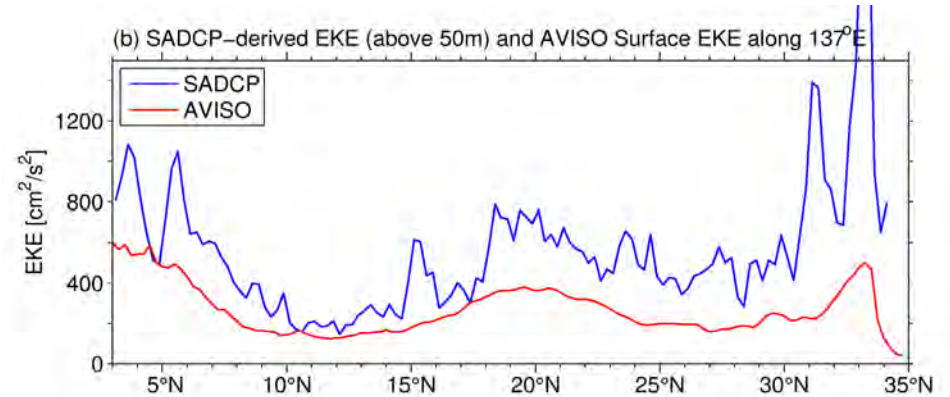
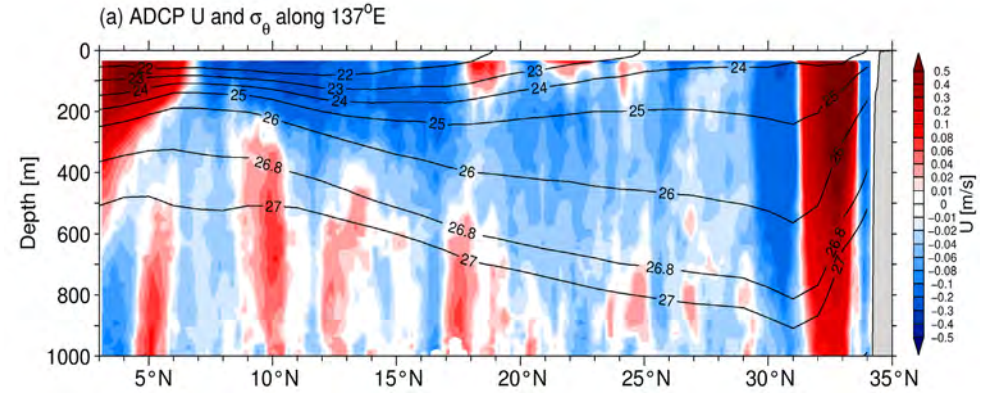
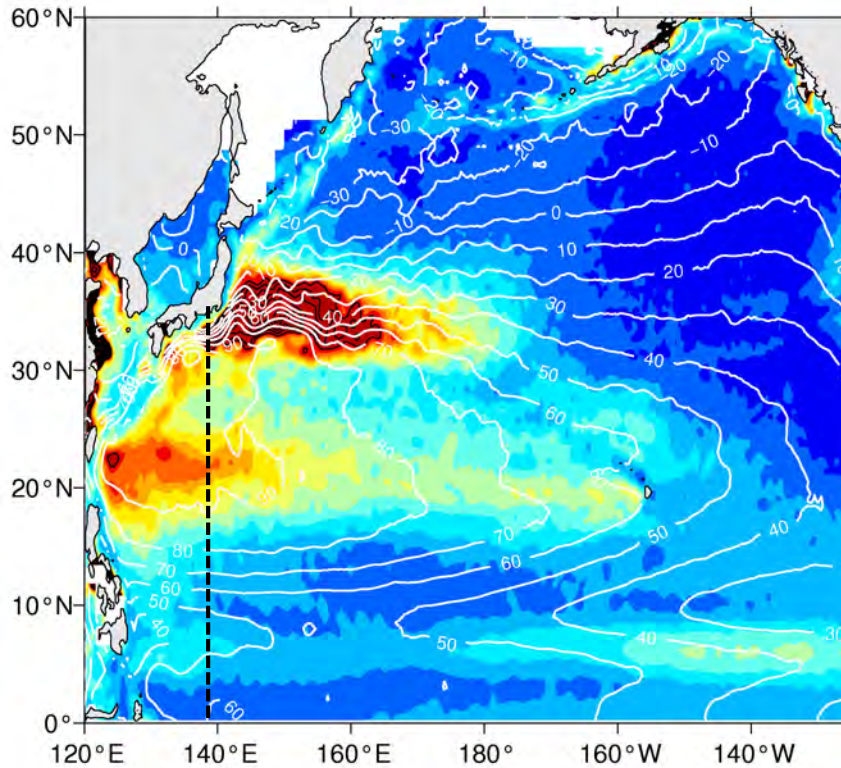
What are missing from the AVISO-derived STCC variability?



R/V Ryofu Maru of JMA

- Repeat ship-board ADCP surveys along 137°E have been carried out by Japan Meteorological Agency
- Analyzed 33 surveys spanning 2004-16
- Upper ocean u/v data (40-1000db) are QC-processed & averaged to a 2.5km grid

Comparison between ADCP- vs. AVISO-derived EKE level

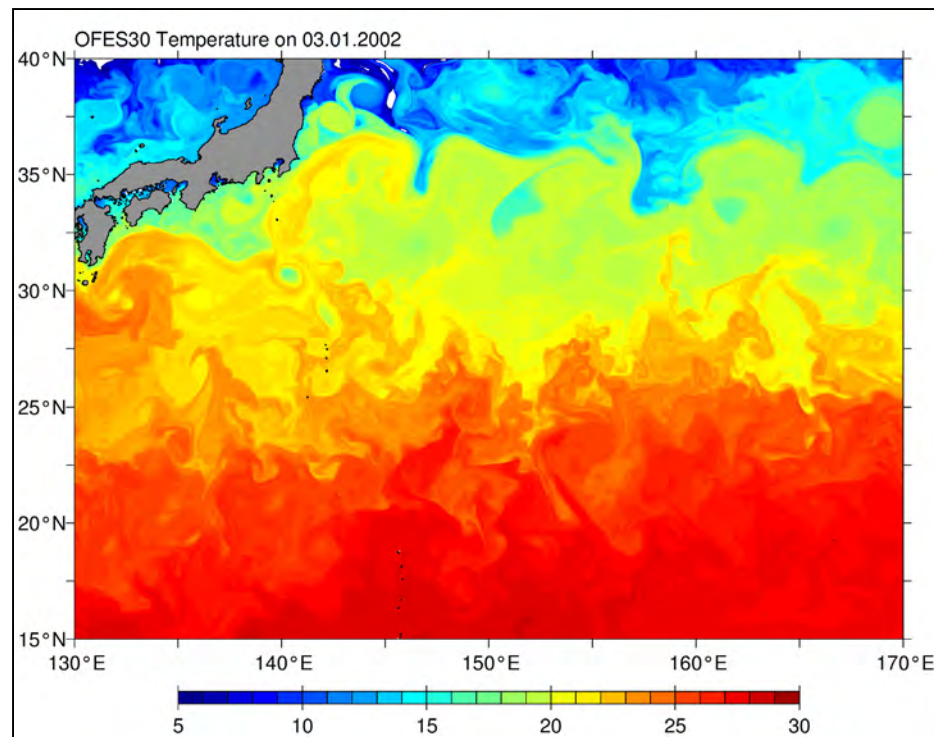
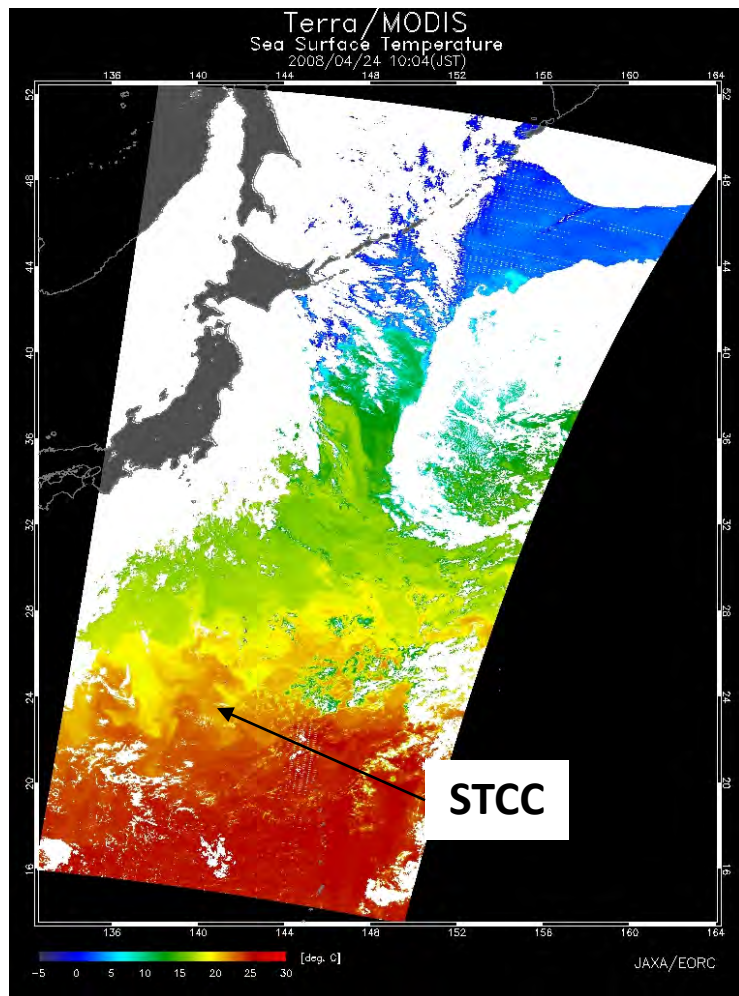


↔ STCC band

- Except for the stable NEC band, AVISO-derived EKE level significantly **under-estimates** the ADCP-derived EKE level

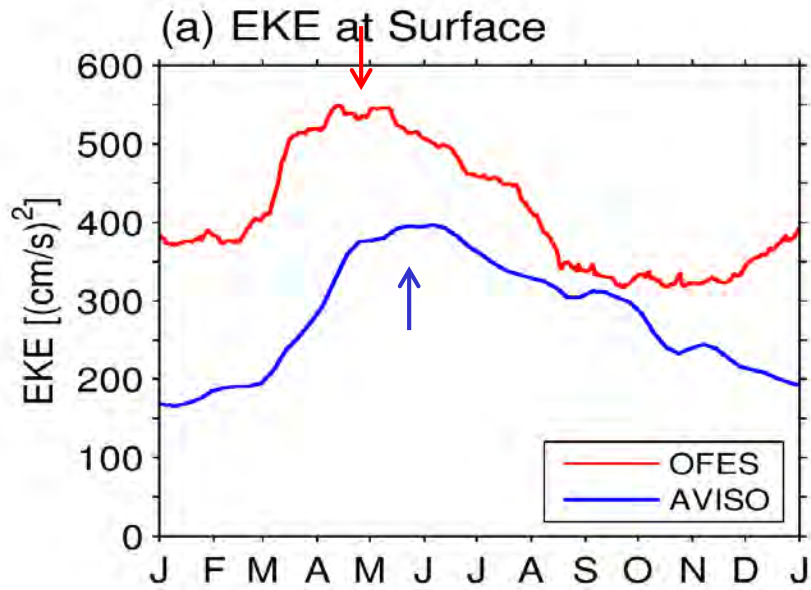
OFES 1/30° N Pacific OGCM Simulation:

- 3-km horizontal grid resolution (100 vertical levels)
- Model domain 100°E-70°W, 20°S-66°N
- Forced by JRA-25 1°x1° 6-hourly reanalysis data



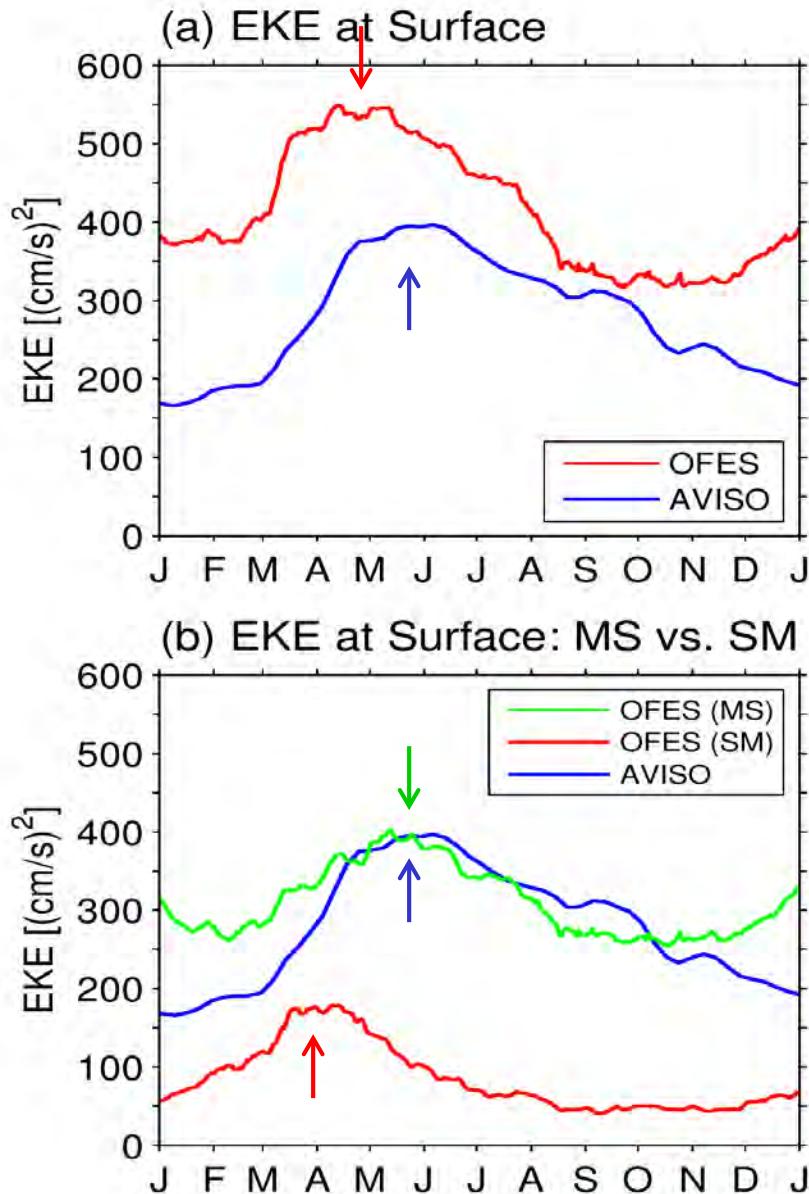
Sasaki, Klein, Qiu & Sasai (2014)

AVISO vs. OFES30 EKE time series in the STCC band: 18°-25°N, 135°-160°E



- Aside from the energy level, modeled EKE peak precedes the AVISO peak by ~1 month

AVISO vs. OFES30 EKE time series in the STCC band: 18°-25°N, 135°-160°E



- Aside from the energy level, modeled EKE peak precedes the AVISO peak by ~1 month

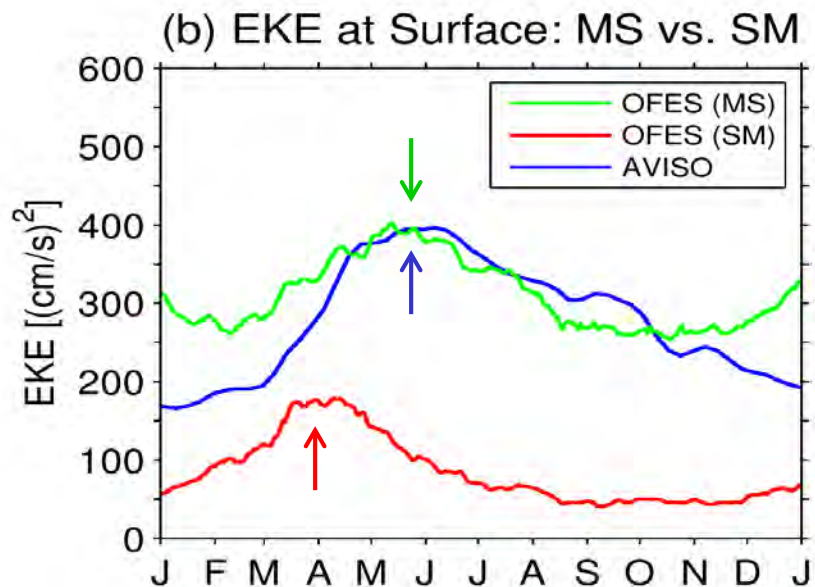
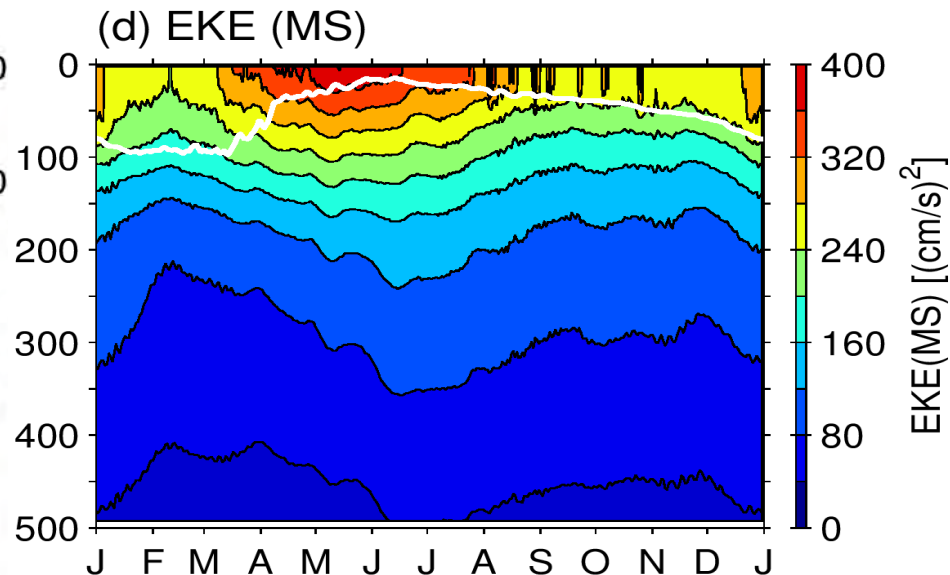
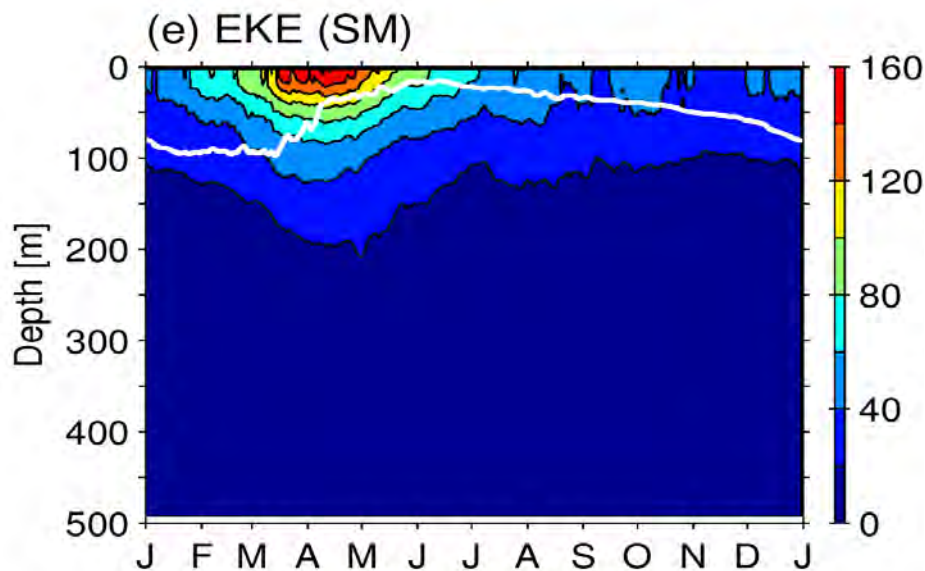
$$\eta' = \eta'_{\text{MS}} + \eta'_{\text{SS}}$$

η'_{MS} : mesoscale SSH signals
resolved by AVISO; $2\pi/K > 150$ km

η'_{SS} : submesoscale SSH signals
unresolved by AVISO; $2\pi/K < 150$ km

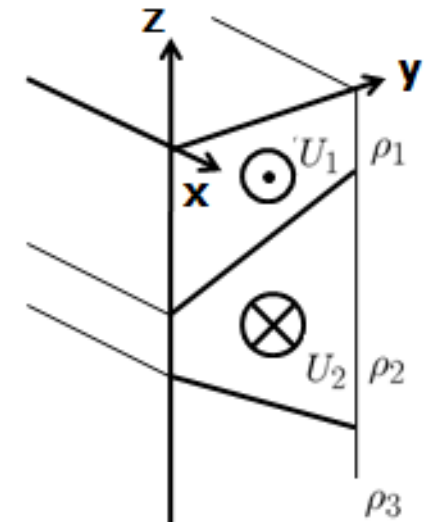
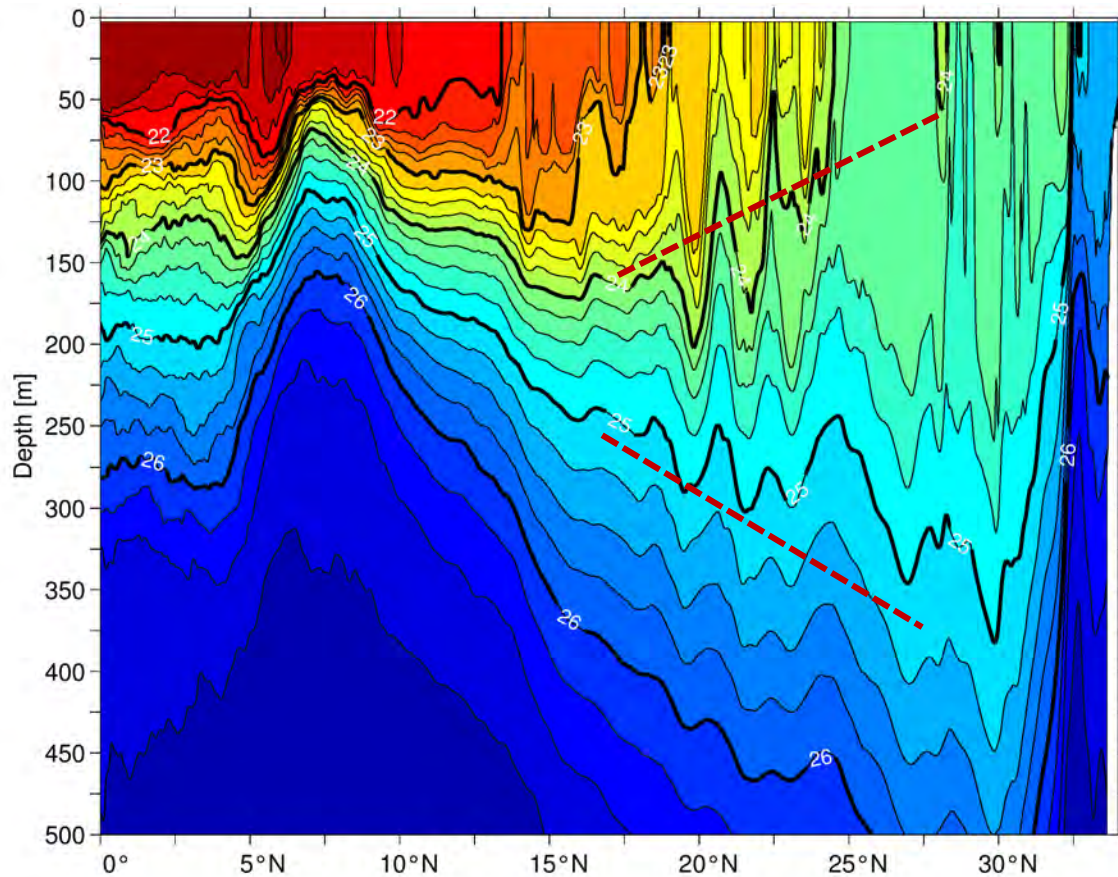
- Mesoscale OFES EKE seasonal amplitude/phase are similar to AVISO
- Submesoscale EKE peaks in late March

OFES30 vertical EKE time series in the STCC band: 18°-25°N, 135°-160°E



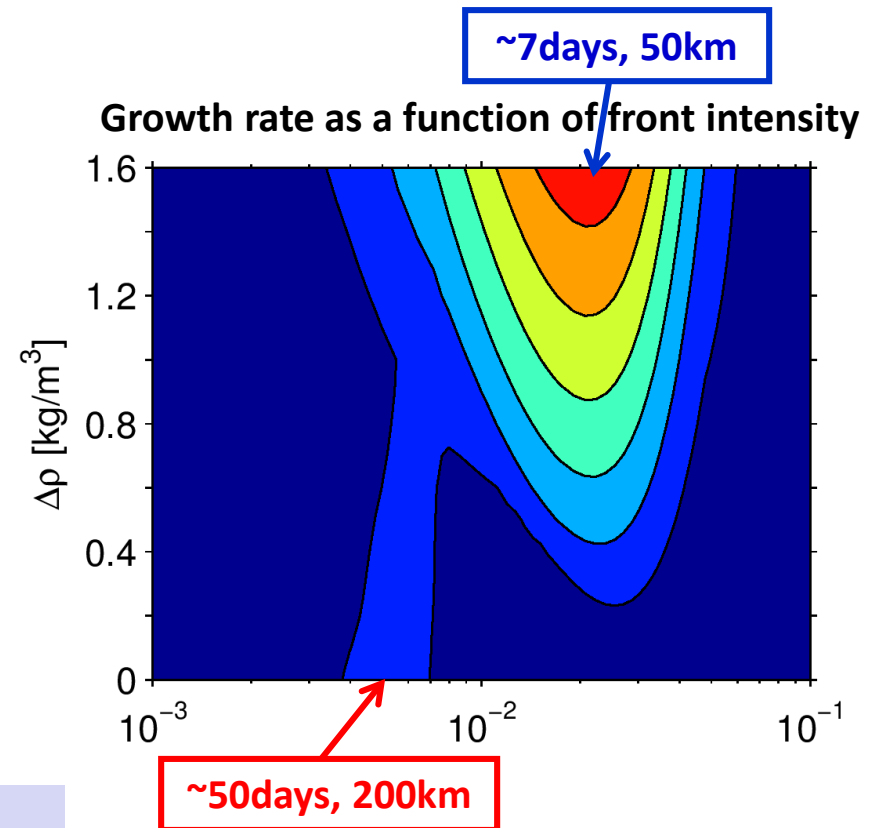
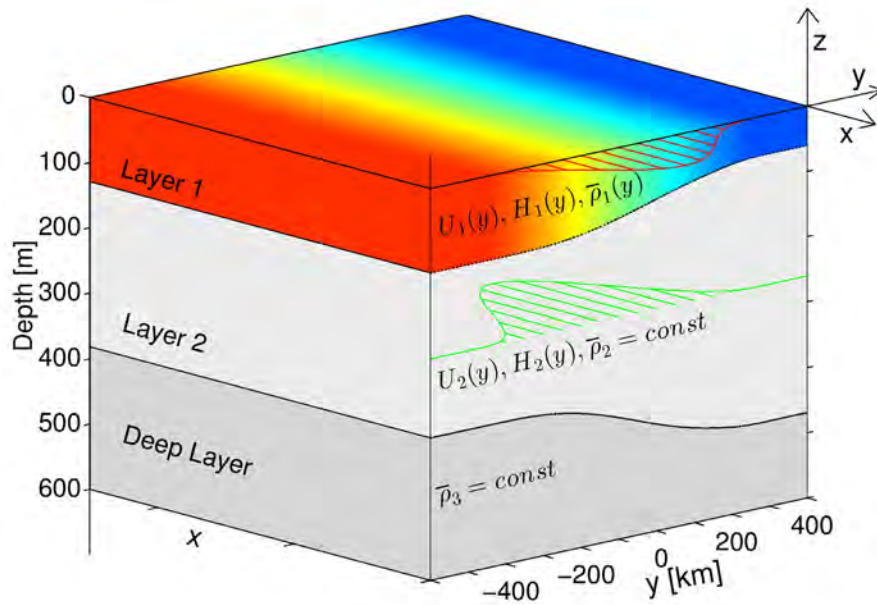
- Vertically, submesoscale EKE is largely trapped within the surface ML (white curve)
- Mesoscale EKE has deeper expressions and its seasonal peak lags with increasing depth

OFES30 $\sigma_\theta(y,z)$ section along 135°E on 1 March 2002



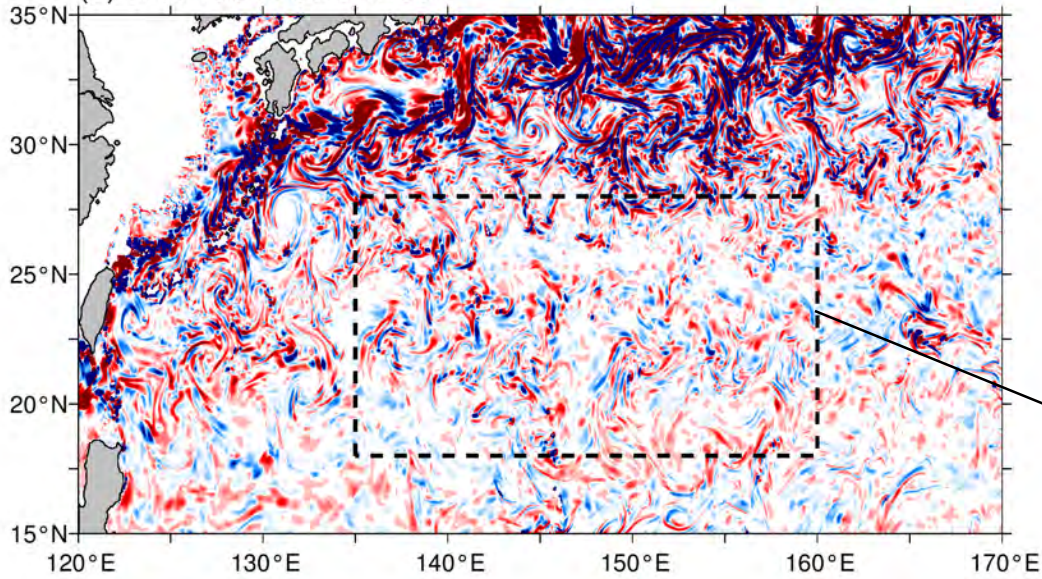
- In addition to the vertical STCC/NEC shear that generates interior baroclinic instability, **steep density gradients in the mixed layer lead to submesoscale ML instability**

An extended 2.5-layer RG model with density front embedded in upper layer



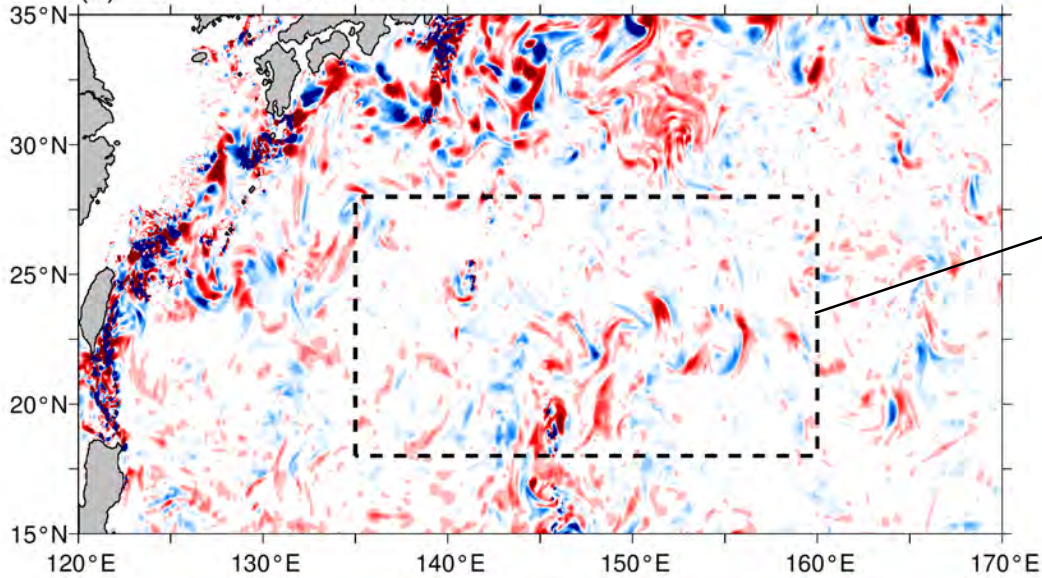
- When $\Delta\rho = 0$ (no upper layer density front), the analysis recovers the interior QG instability
- When $\Delta\rho \neq 0$, ML frontal instability occurs
- ML instability has faster growth rate & shorter most unstable wavelength

(a) w at 100m: 03/01/2001

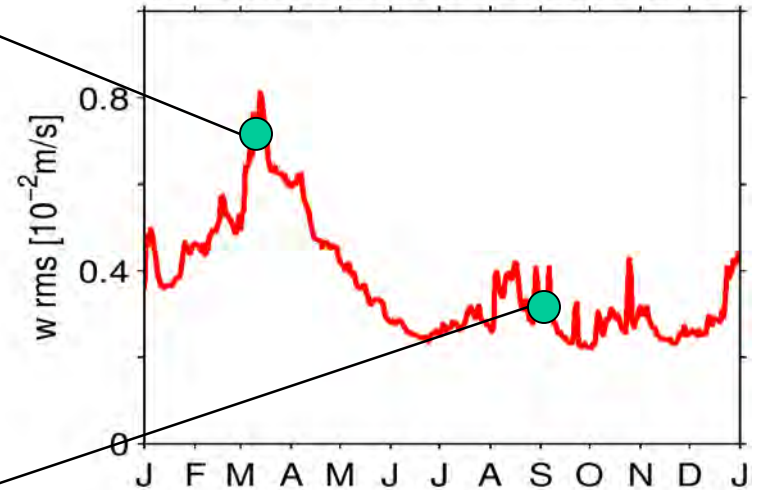


Instantaneous 100m vertical velocity maps from the 1/30° OFES: March vs. September

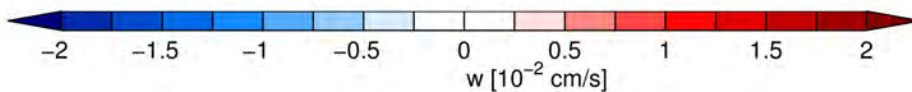
(b) w at 100m: 09/01/2001



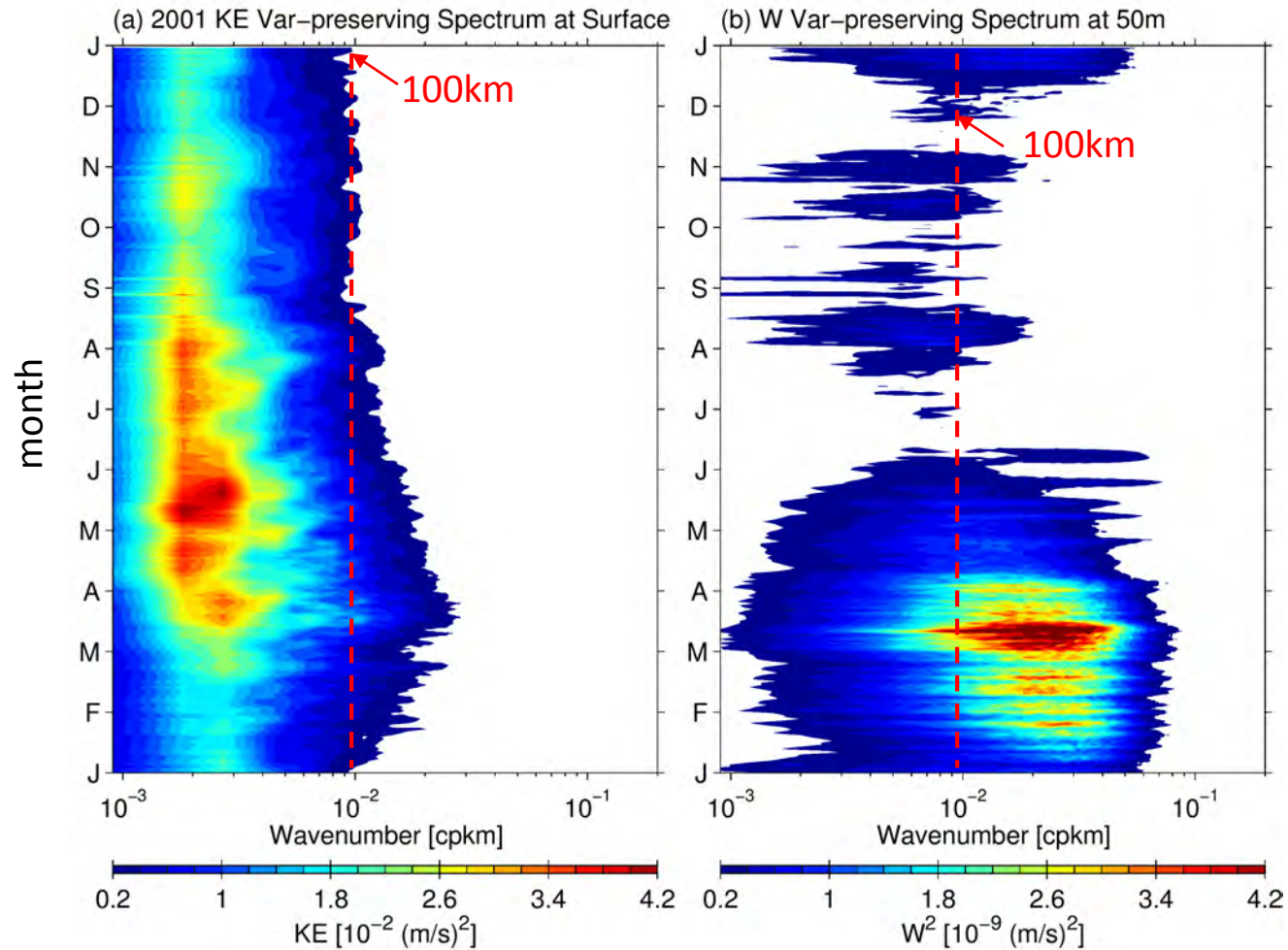
(a) w rms Timeseries at 100m



• Submesoscale variability controls the w signals!

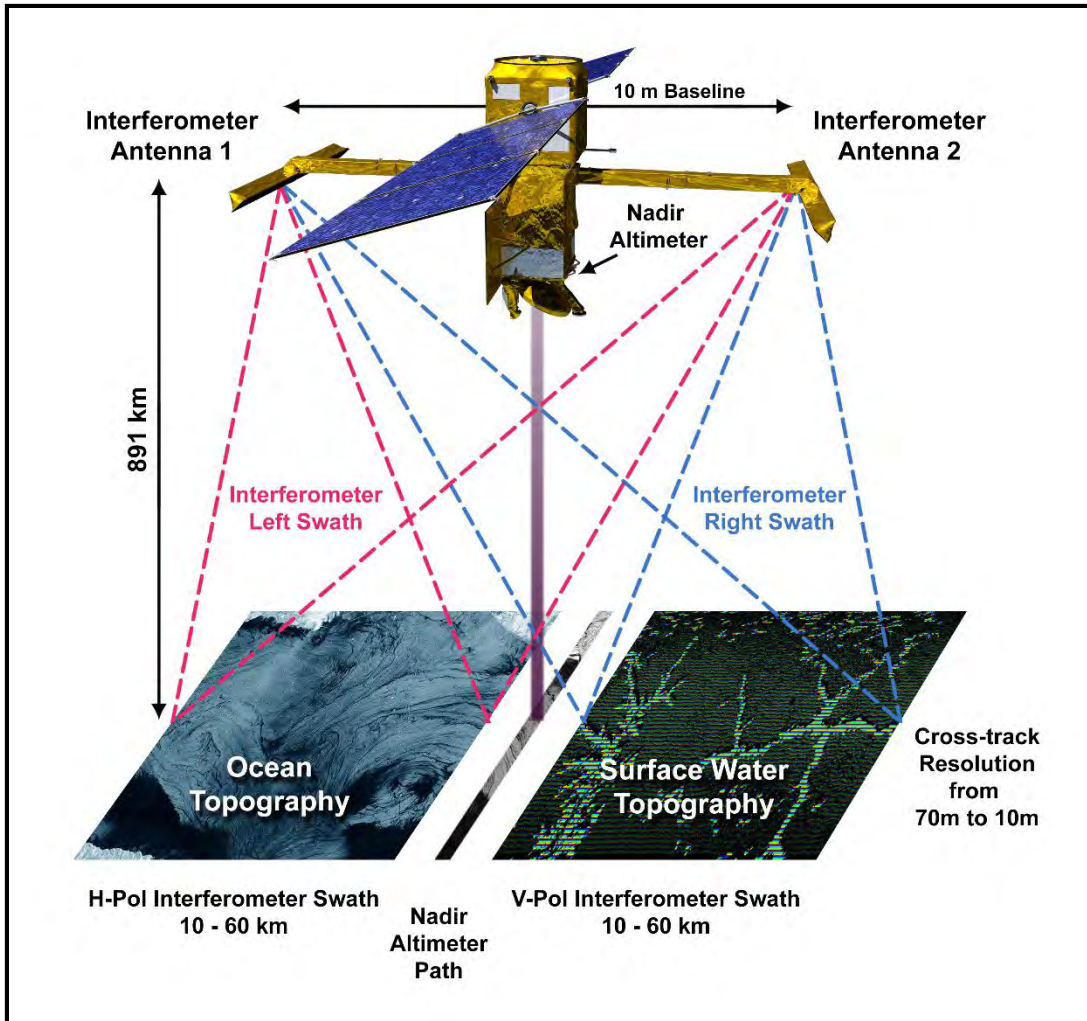


OFES30 horizontal ($z=0$) vs. vertical velocity ($z=50\text{m}$) spectra



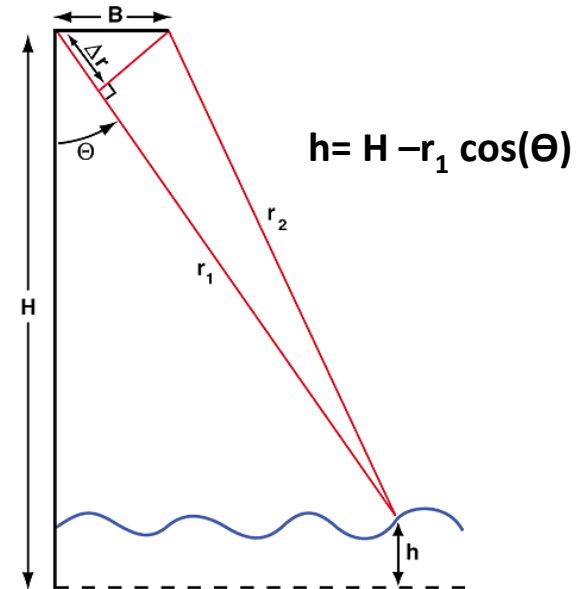
- While mesoscale eddy variability controls the horizontal circulation changes, **submesoscale variability** controls the **w amplitude/seasonality**

NASA-CNES Surface Water and Ocean Topography (SWOT) Mission



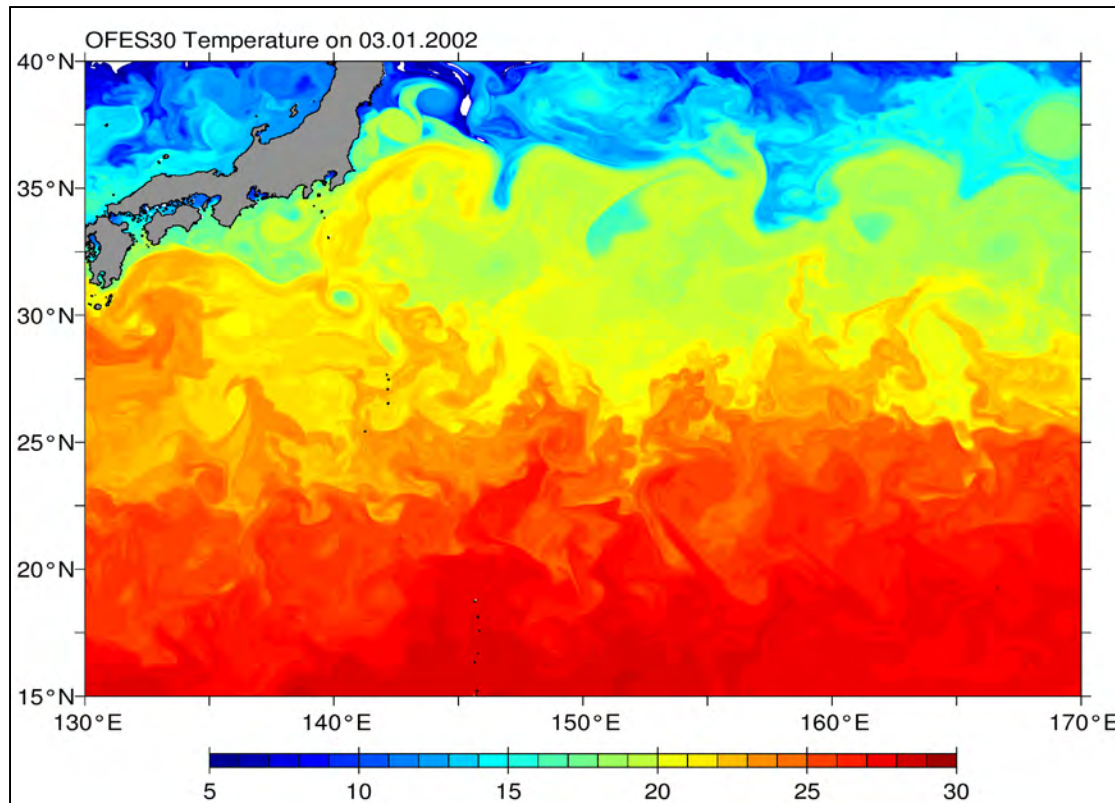
<https://swot.jpl.nasa.gov>

- Point vs **120km-wide swath** measurements
- $O(150\sim 200\text{km})$ vs **$O(15\text{km})$** resolution; cf. $L_R = O(50\text{km})$
- Planned launch: **Sept. 2021**
- Ka-band radar **Interferometer** measurement (see below)

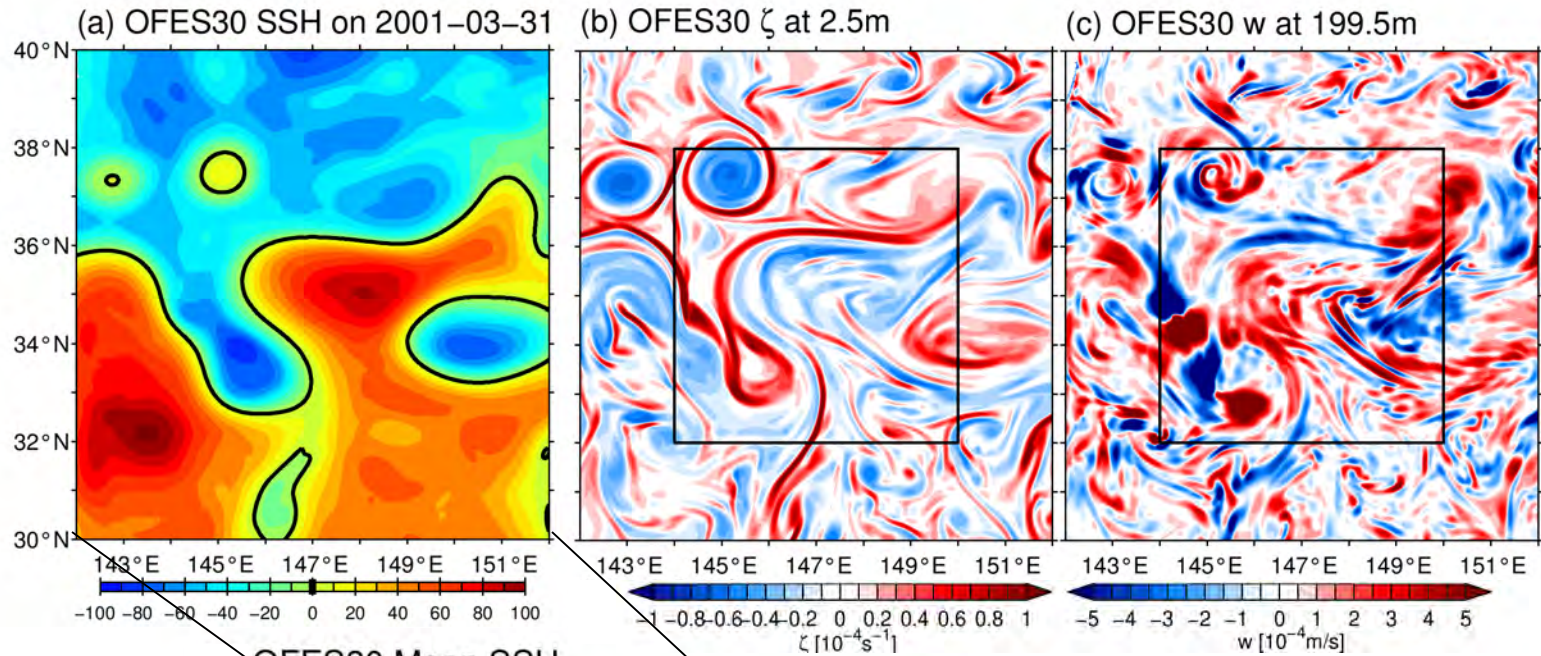


Opportunities from the SWOT Mission: an Example

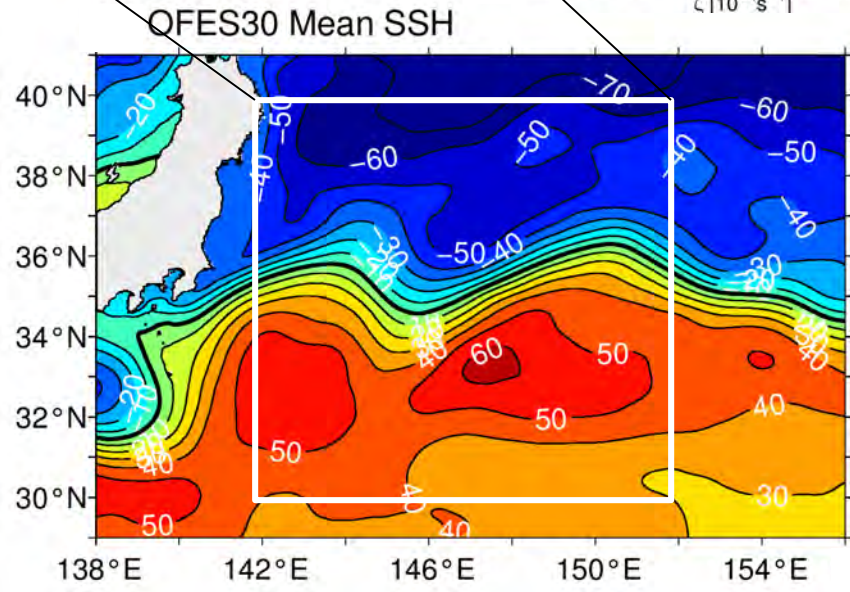
- Submesoscale features tend to be advected by the mesoscale circulation in which they're imbedded
- This opens the possibility of reconstructing the 3D upper ocean circulation structures, including w field, using the high-resolution SSH data from SWOT



Case study in the Kuroshio Extension region: March 31, 2001



OFES
original



Input: 10°x10° SSH η field (upper left)

Target: 6°x6° relative vorticity ζ field (upper middle)

6°x6° vertical velocity w field (upper right)

(a smaller target box is chosen to avoid edge effect)

Effective surface quasi-geostrophic (SQG) theory: Lapeyre and Klein (2006)

- Under the assumption that surface & subsurface PV anomalies are correlated, the geostrophic streamfunction anomaly ψ can be functionally related to the SSH anomaly η by :

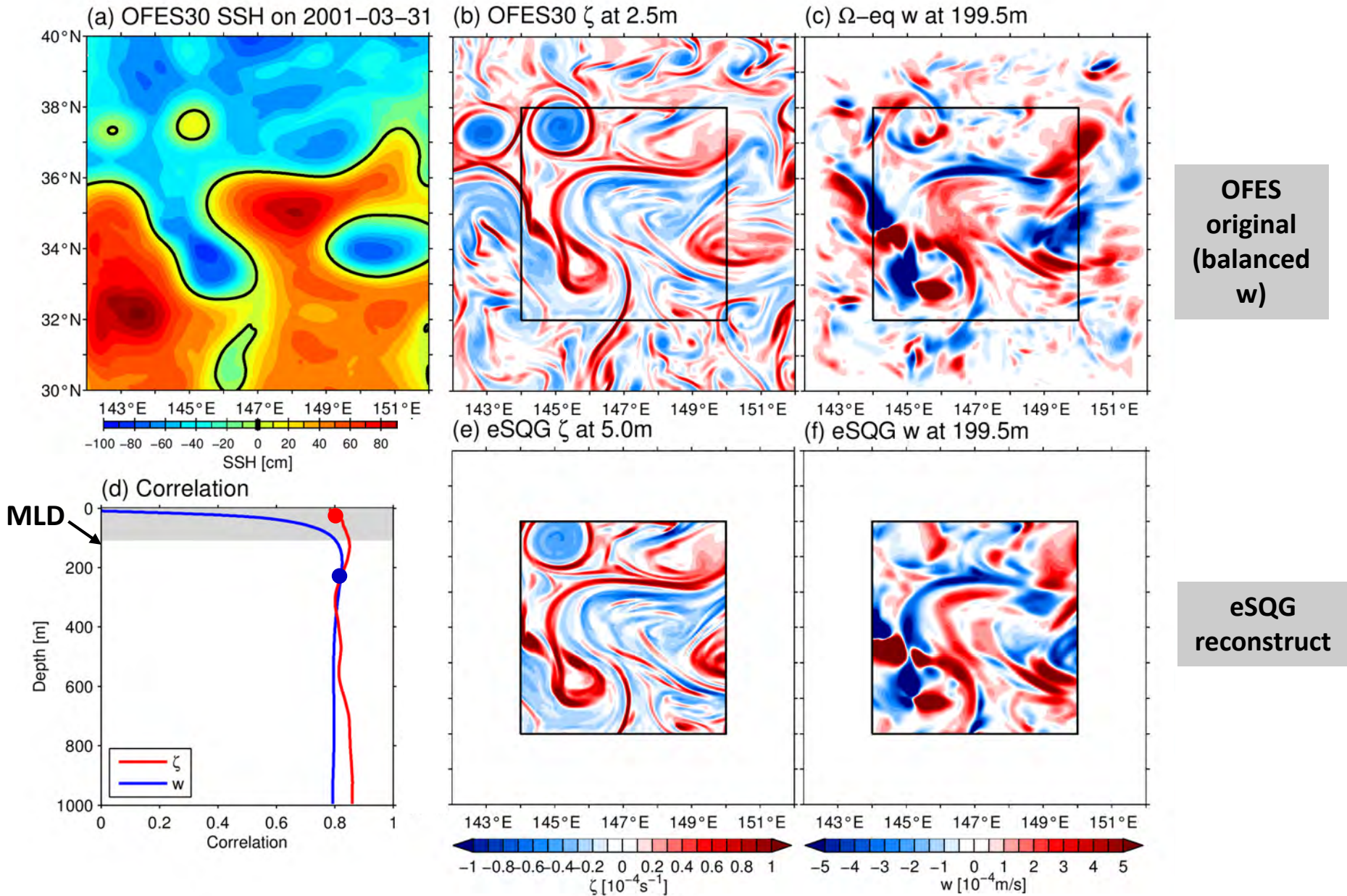
$$\hat{\psi}(\mathbf{k}, z) = \frac{g}{f_o} \hat{\eta}(\mathbf{k}) \exp\left(\frac{N_o}{f_o} k z\right)$$

where $\hat{\cdot}$: horizontal Fourier transform, \mathbf{k} : horizontal wavenumber, and N_o : effective buoyancy frequency.

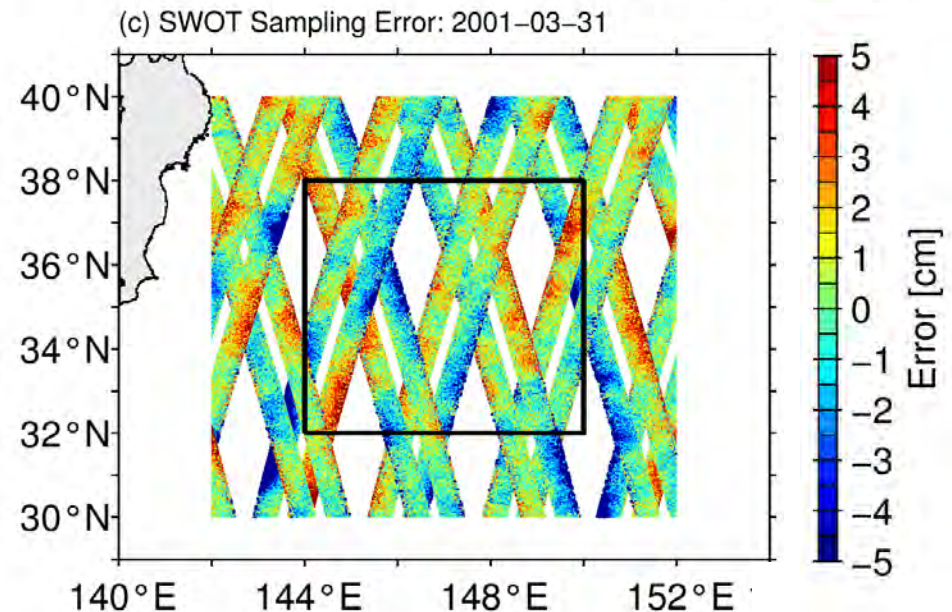
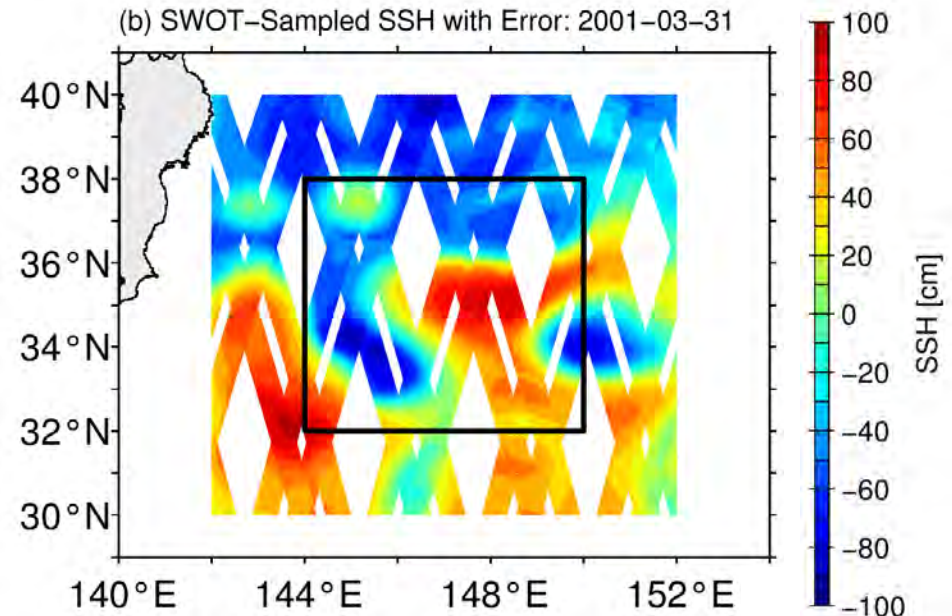
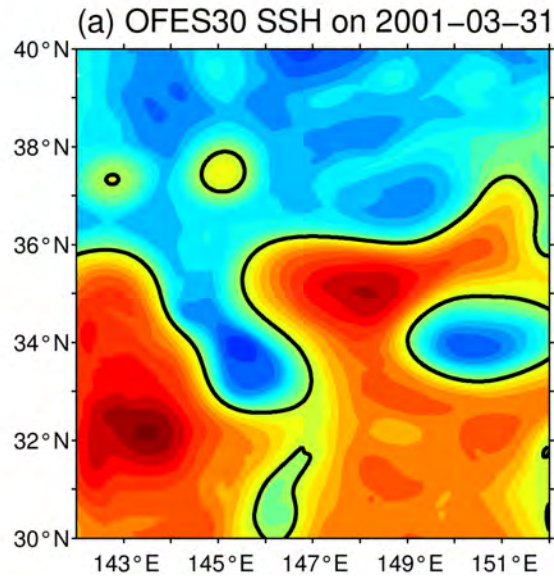
- Once ψ is specified, 3-D fields of relative vorticity, buoyancy, & vertical velocity can be deduced from geostrophy, hydrostaticity, & advective buoyancy equation, respectively :

$$\begin{aligned}\hat{\zeta}(\mathbf{k}, z) &= -k^2 \hat{\psi}(\mathbf{k}, z), \\ \hat{b}(\mathbf{k}, z) &= \frac{N_o k}{c} \hat{\psi}(\mathbf{k}, z), \\ \hat{w}(\mathbf{k}, z) &= -\frac{c^2}{N_o^2} \left[-J(\widehat{\psi_s}, b_s) \exp\left(\frac{N_o}{f_o} k z\right) + J(\widehat{\psi}, b) \right]\end{aligned}$$

Best reconstruction: modeled η as input, no swath gaps/measurement errors

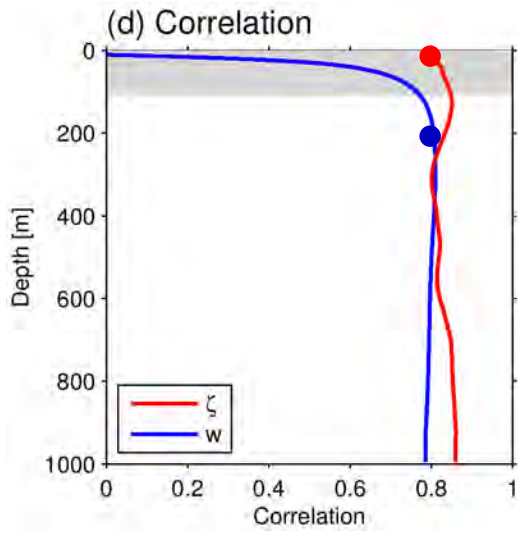


SWOT simulator-sampled SSH field in a sub-cycle centered on March 31

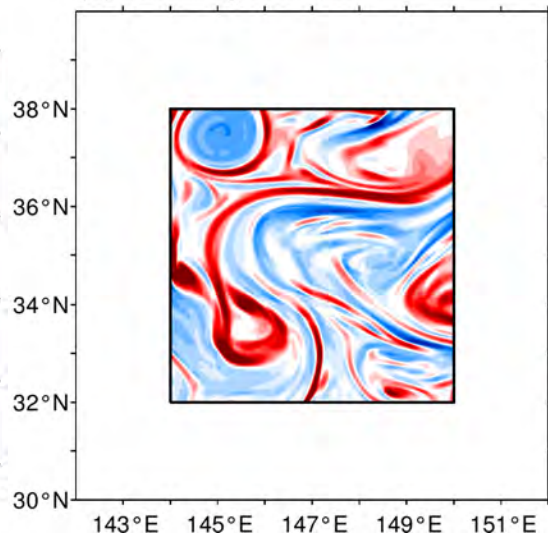


- Spatial η discontinuities due to swath time difference and larger measurement errors toward edges
- Measurement errors have a larger impact on small-scale η signals due to larger noise-to-signal ratio

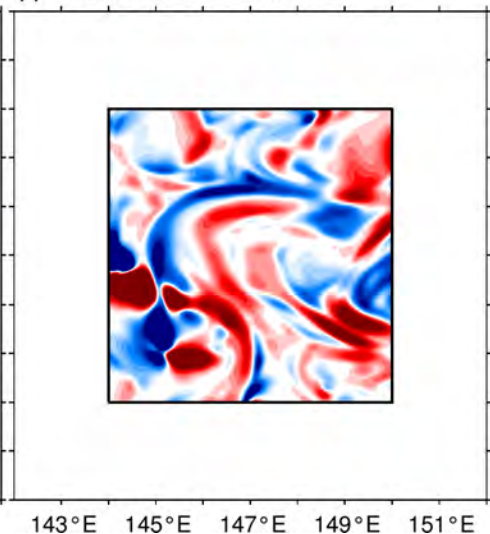
Reconstruction comparisons with simulated vs. mapped SSH field as input



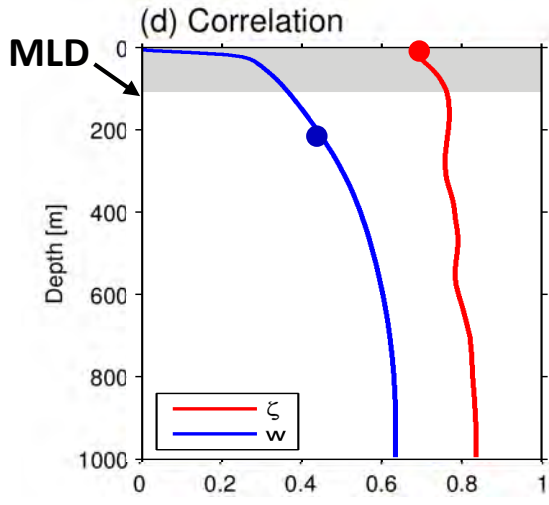
(e) eSQG ζ at 5.0m



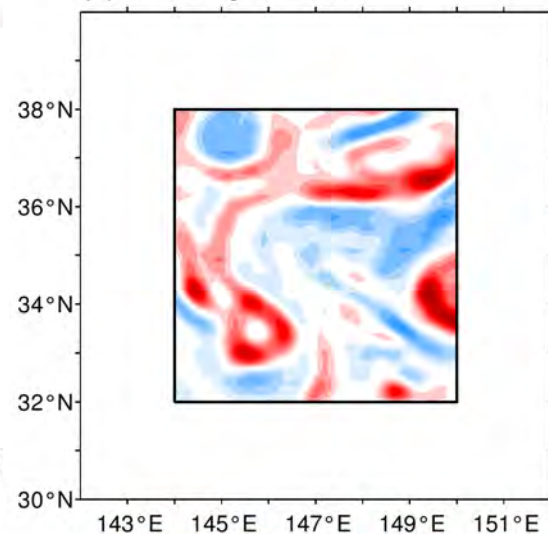
(f) eSQG w at 199.5m



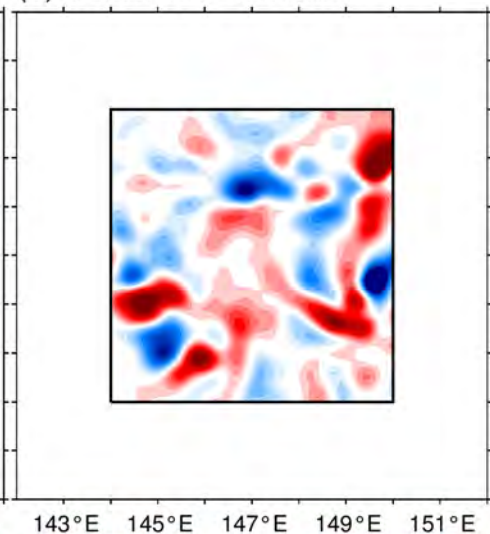
eSQG
original
reconstruct



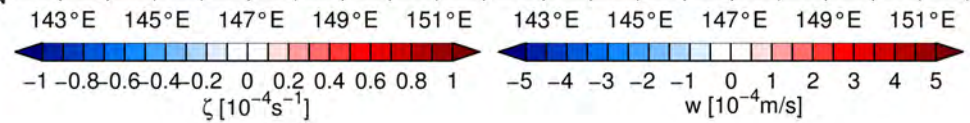
(c) eSQG ζ at 5.0m



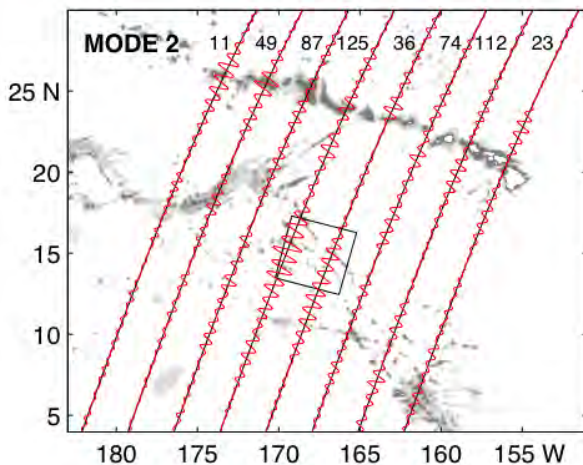
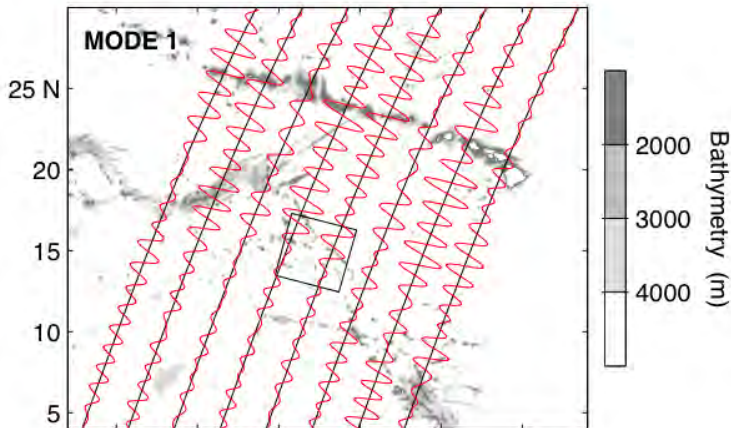
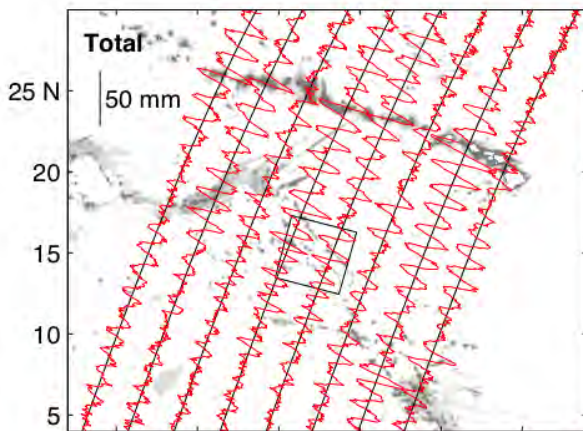
(d) eSQG w at 199.5m



eSQG
SWOT
reconstruct



Qiu et al.
(2016, JPO)

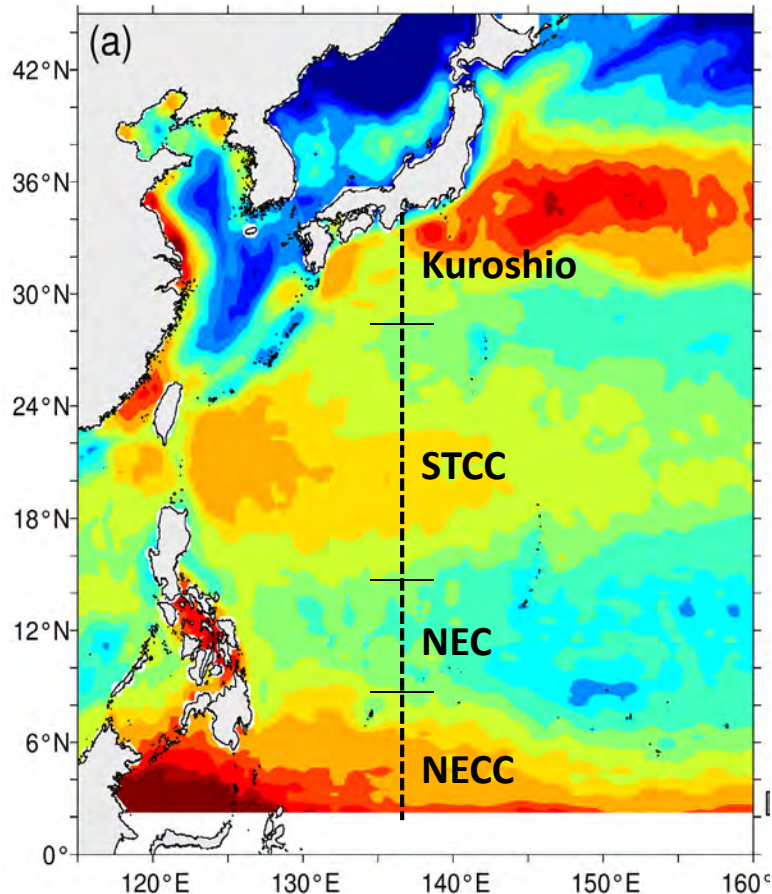


- SSH signals associated with the **coherent M_2 internal tides** around Hawaiian Islands
- Mode-1 has a wavelength of **$\sim 150\text{km}$** & an amplitude of **$\sim 5\text{cm}$**

Challenges

- For mesoscales with $2\pi/k > 150\text{km}$, balanced geostrophic flow dominates and altimeter-derived SSH can be readily used to infer surface geostrophic velocities
- As the geostrophic flow weakens as $k^{-2} \sim k^{-3}$, unbalanced wave motions can overtake in the 10-150km meso-submesoscale range
- For SWOT mission, it is important to identify the length scale **Lt** at which **geostrophic flow** loses its dominance & is overtaken by unbalanced **wave motions**

JMA repeat S-ADCP surveys along 137°E

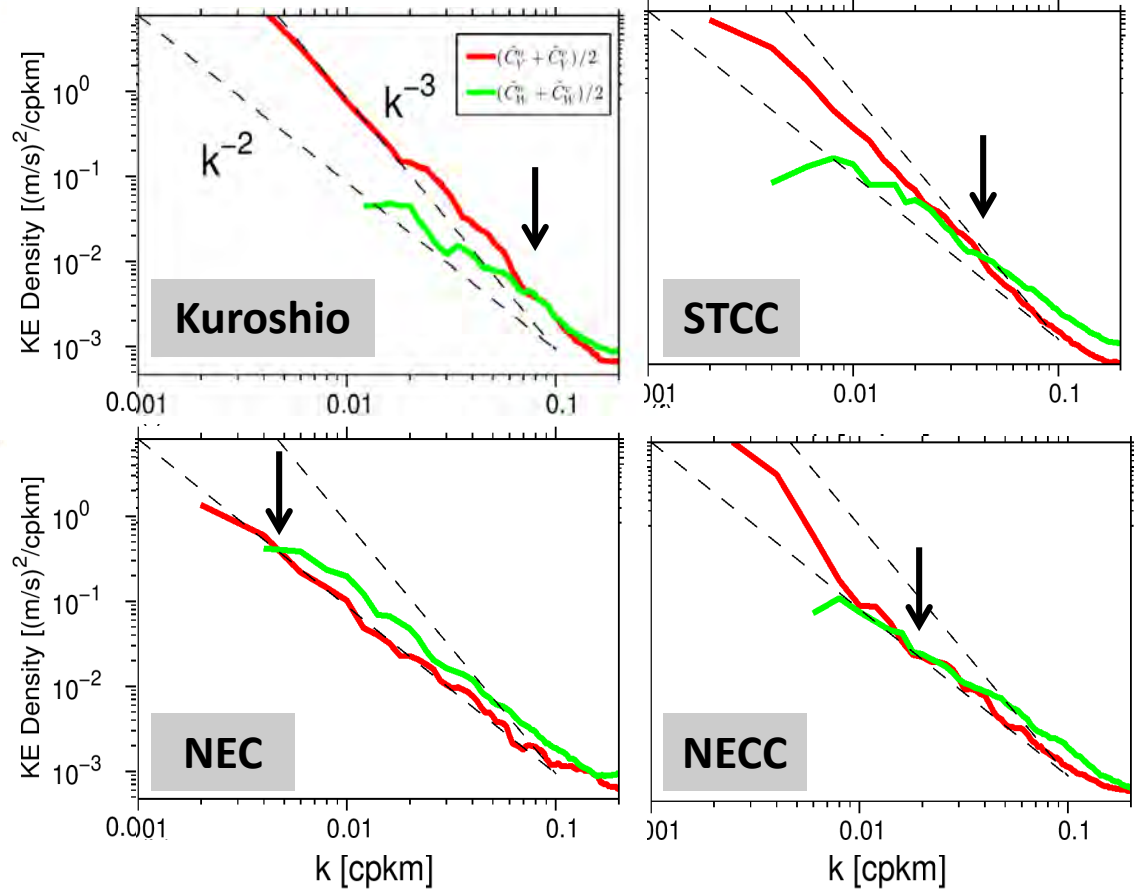
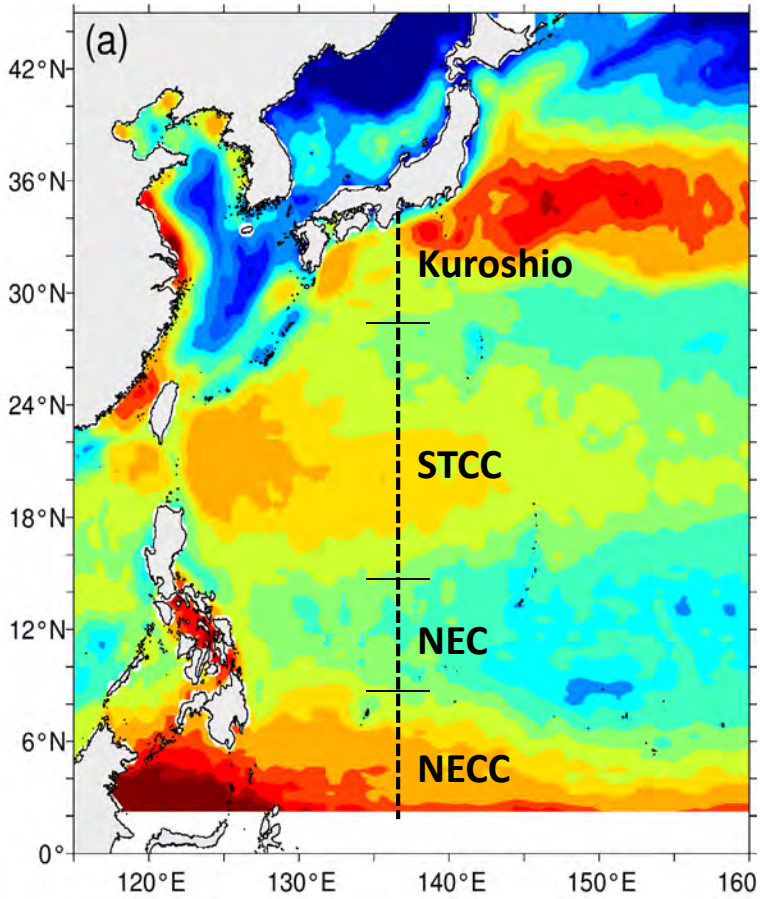


Separating balanced vs. unbalanced motions:

- Under isotropic condition, Helmholtz decomposition allows $(u, v) = (-\psi_y + \phi_x, \psi_x + \phi_y)$ be separated into rotational ψ & irrotational ϕ components. In spectral space:
 $S^u(k), S^v(k) \rightarrow S^\psi(k), S^\phi(k)$ (Bühler et al. 2014)
- By definition, geostrophic flow has ψ only (i.e., $S^\phi_g(k) = 0$) & KE spectrum for ϕ is completely set by wave motions: $S^{\phi_w}(k) = S^\phi(k)$
- Assuming internal waves in open ocean follow the Garrett-Munk spectrum, rotational part of $S^\psi(k)$ for the internal waves becomes: $S^{\psi_w}(k) = f^2 S^{\phi_w}(k) / \omega_*^2$
- Given $S^{\psi_w}(k)$, geostrophic KE spectrum is
 $S^{\psi_g}(k) = S^\psi(k) - S^{\psi_w}(k)$
- Transition scale L_t is defined at where
 $S^{\psi_g}(k) = S^{\psi_w}(k) + S^{\phi_w}(k)$

JMA repeat S-ADCP surveys along 137°E

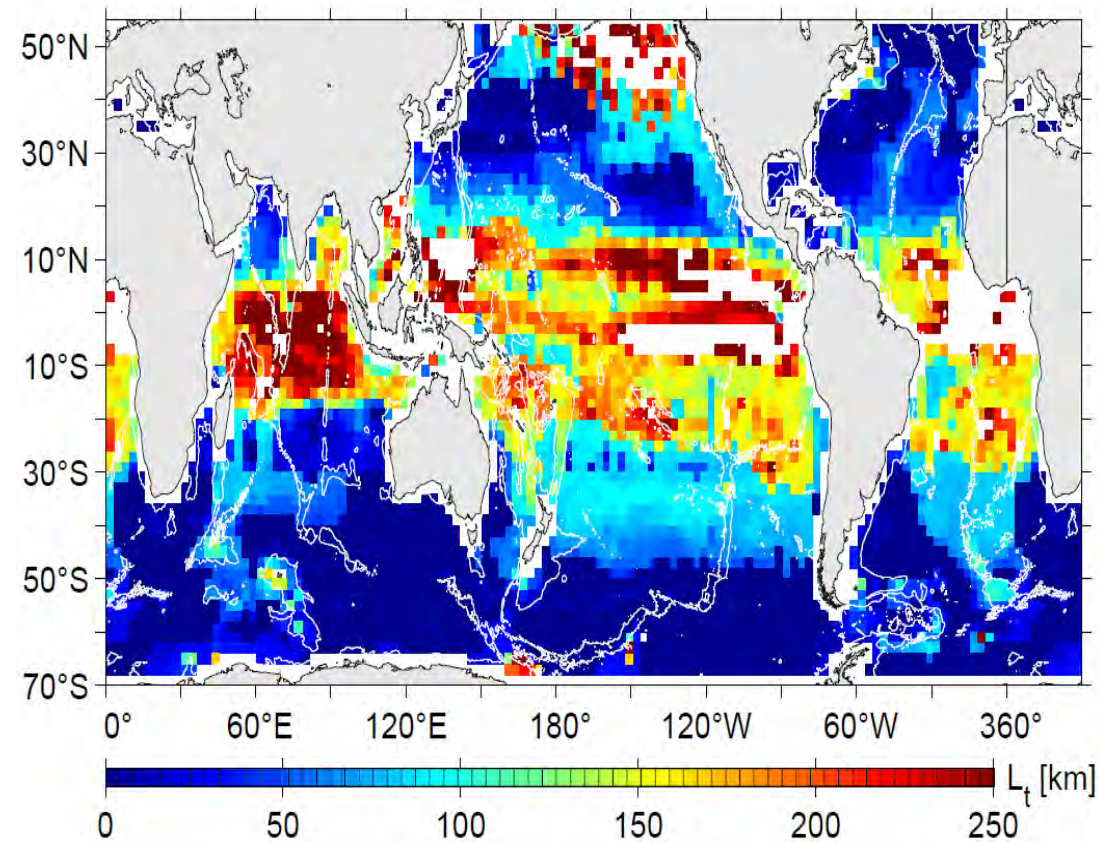
- **Kuroshio: $L_t = 12\text{km}$**
- **Subtropical Countercurrent: $L_t = 25\text{km}$**
- **North Equatorial Current: $L_t = 250\text{km}$**
- **North Equatorial Countercurrent: $L_t = 80\text{km}$**



Qiu et al. (2017, Nat Com)

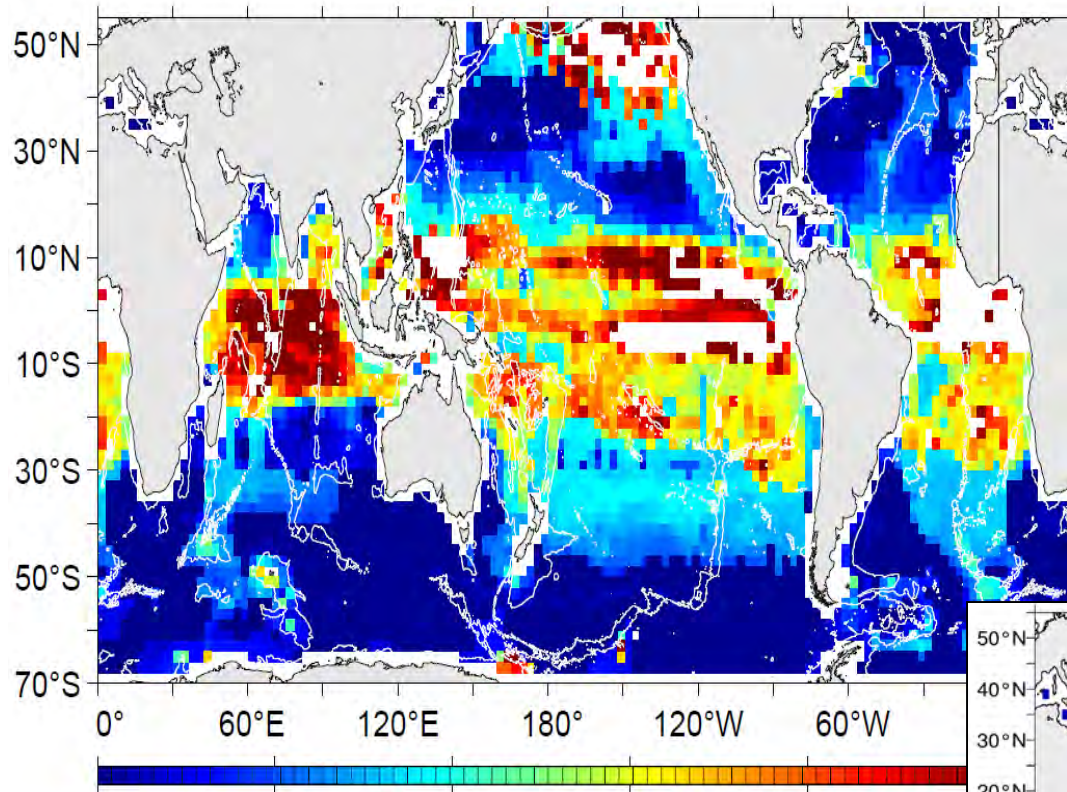
KE spectra for **geostrophic** vs. **wave motions**

Global L_t inferred from 1/48° MITgcm

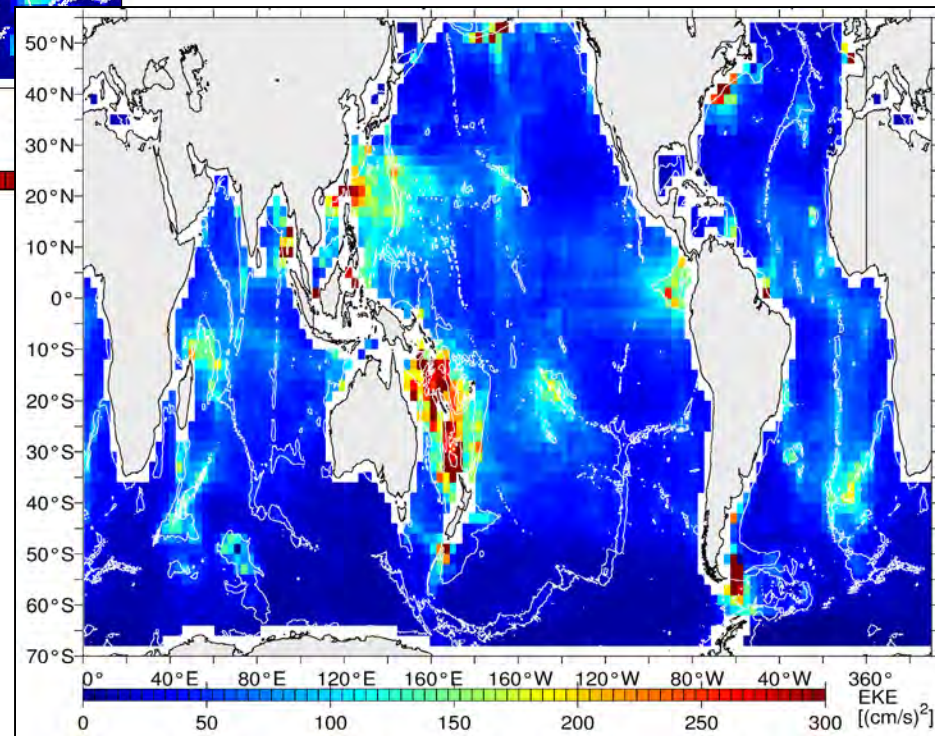


- Consistent with ADCP estimates in NW Pacific
- Globally, $L_t < 30\text{km}$ in WBC regions & ACC; exceptions appear in EAC & in ACC areas with prominent topographic features
- In temperate latitudes (i.e., STCC bands), $L_t = 50\sim 100\text{km}$
- $L_t > 150\text{km}$ in most of tropics & the Alaskan Gyre

Global L_t inferred from 1/48° MITgcm



EKE level of unbalanced wave motions



- Regional mesoscale eddy variability is only **one determinant** for L_t
- Energy level for unbalance wave motions is **spatially non-uniform**; it affects L_t in regions like EAC & along ACC path

Qiu et al. (2018, JPO)



Concluding Remarks

- Current altimetry measurements only capture mesoscale variability with spatial scales $> 150\text{km}$
- Interior and ML baroclinic instabilities occur concurrently along STCC. Interior instability is deep-reaching, slowly-growing & controls the seasonal evolution of horizontal KE field
- ML instability is confined to wintertime ML, fast-growing & diminishes after April. It generates submesoscale variability & dictates the seasonal evolution of w field
- SWOT SSH measurements have the potential to allow us to infer the 3D upper ocean circulation, including w field, on a repetitive & global scale
- Disentangling the balanced geostrophic & unbalanced wave motions in the SWOT-measured, submesoscale-resolving, SSH data poses a challenge